DAMAGE LOCALIZATION OF SLAB-ON-GIRDER BRIDGES THROUGH VIBRATION CHARACTERISICS

A Thesis
Submitted to the Graduate Faculty
of the
North Dakota State University
of Agriculture and Applied Science

By

Michael Andrew Telste

In Partial Fulfillment of the Requirements
for the Degree of
MASTER OF SCIENCE

Major Department:
Civil and Environmental Engineering

March 2015

Fargo, North Dakota

North Dakota State University
Graduate School

Title

Damage Localization of Slab-on-Girder Bridges Through Vibration Characteristics

By

Michael Andrew Telste

The Supervisory Committee certifies that this ***disquisition*** complies with North Dakota State University's regulations and meets the accepted standards for the degree of

MASTER OF SCIENCE

SUPERVISORY COMMITTEE:

Dr. Mijia Yang
Chair

Dr. Ying Huang

Dr. Frank Yazdani

Dr. Jerry Gao

Approved:

4/13/2015
Date

Dr. Dinesh Katti
Department Chair

ABSTRACT

An incompletely documented bridge 09-125-16 in Cass County, ND was tested by Bridge Diagnostics, Inc. (BDI). A Grillage numerical model is created with their field data to simulate the bridge responses due to traffic loads. A validated bridge model matching the field test data is developed.

Based on the validated numerical model, loading of the corresponding bridge under different damage scenarios is performed to capture the change of displacement mode shapes. Using the difference of these displacement mode shape data, a modified curvature method is suggested for identifying damage in bridges, which is shown successfully through the modeling results of bridges with fictitious damages. An in-lab experiment of a steel plate without damage under impact forces is adopted to produce vibration data. The modified curvature is then computed using the experimental mode shape data and its change is found to correlate very well as anticipated by the suggested theory.

TABLE OF CONTENTS

LIST OF TABLES

LIST OF FIGURES

1. INTRODUCTION

1.1. Background

U.S. bridge infrastructure has recently received a grade of C+ in ASCE's 2013 Report Card for America's Infrastructure. The report card stated that 1 in 4 bridges across the United States are either 'structurally deficient' or 'functionally obsolete' or both. In addition, the average age of a bridge is 42 years and 30% of existing bridges have exceeded their 50-year design life (American Society of Civil Engineers, 2013). An aging infrastructure requires developing ways to efficiently address critical need areas with finite resources.

Structural health monitoring (SHM) is a promising research field for addressing the issues stated above. This thesis will focus on SHM applied to bridge structures.

There are several goals that a structural health monitoring systems can achieve. SHM can provide increased understanding of in-situ structural behavior. Damage detection is another important goal in SHM, and determination of strength and remaining service life and assistance in infrastructure management.

The basic structural health monitoring system involves applying a single type of sensor or multiple types of sensors, depending on what data is desired. The sensor data is then collected and processed by various data processing systems and strategies. This processed data is then evaluated by technicians or engineers who then interpret the data to determine if any information about the monitored structure can be revealed. There are several types of monitoring strategies that have been used in research. Some of these are static loading testing, dynamic testing, periodic monitoring, and continuous monitoring. Each of these strategies can be tailored to accomplish certain goals set by the owner or the researcher.

Even though bridge health monitoring technology has been researched for more than 10 years, it still poses severe problems in correlating with damage types and conditional rating of bridges. In this thesis, four important aspects in bridge health monitoring technology will be explored: (1) Ambient excitation using traveling traffic (not to be able to be implemented in this thesis due to time); (2) Benchmark base line data provided by advanced modeling; (3) Improved damage index to correlate with bridge status and rating; and (4) Verify the concepts through experiments.

1.2. Ambient Excitation for Bridge Health Monitoring Using Traveling Traffic

Dynamic based bridge health monitoring uses either designated excitation or ambient excitation. Ambient excitation typically is more appealing due to its convenience, however data noise is introduced and necessitates complicated signal processing.

Designated excitation, such as free and forced vibration tests as well as shake table tests, have been conducted through the years for assessing structural status of bridges. Hudson conducted a full scale bridge experiment and mode shapes obtained from those of forced-vibration tests were presented (Hudson, 1977). Srinivasan, et al. reviewed a large number of dynamic tests performed on as-built nuclear power plant buildings. The types of structures tested varied widely ranging from box-like reactor buildings to a spherical steel containment shell. Loading on the various nuclear power plant structures also varied widely: steady-state forced vibrations; impulsive loading with rockets; impulse/seismic simulation with buried explosives; and free vibrations resulting from step-relaxation tests (Srinivasan, Kot, Hsieh, & Chung, 1981).

Ambient vibrations in bridges may be caused by traffic, wind, water waves, seismic ground motions or other environmental factors. These vibrations can be characterized in terms of the resonant frequencies, mode shapes, and damping of the lower modes of the structure.

One difficulty with determining the dynamic parameters of a structure undergoing ambient vibrations is that the forcing function is not precisely characterized, ruling out conventional FRF spectral analysis techniques, which requires the measurement of the forcing function.

The first attempt at fully characterizing the dynamic parameters of a bridge undergoing ambient vibrations is due to McLamore, et al., using an extension of a spectral technique developed by Crawford and Ward (Ward & Crawford, 1966). In this work, the recorded motion of the bridge was measured with a series of seismometers. The power spectrum density (PSD) of each recorded motion provided estimates of resonant frequencies and modal damping (McLamore, 1971).

Los Alamos National Lab adopted one bridge on I-40 to perform Structural Health Monitoring (Farrar & Jauregui, 1996). In the report, change of natural frequencies and modal shapes of the bridge under ambient excitation have been discussed and used to locate the damage.

Nichols explored the role of ambient excitation and empirical modeling in detecting damage in offshore structures. Two simple models of an articulated offshore structure are excited using an output of a stochastic process conforming to the Pierson–Moskowitz wave distribution. Based on the structure's response to this excitation empirical phase space models are constructed and damage is demonstrated to be effectively located (Nichols, 2003).

Hillis and Courtney investigated the use of the bicoherence function of measured structural acceleration to provide automatic early detection of damage in an offshore structure. The method is shown to be insensitive to typical operating parameter variations and to variations in wave excitation force. It is demonstrated that very small changes in stiffness of individual

structural members are detectable from measurements of global structural motion (Hillis & Courtney, 2011).

Dohler et. al. studied structural health monitoring with statistical methods during progressive damage test of S101 Bridge. In the on-site test, ambient vibration data of the S101 Bridge was recorded while different damage scenarios were introduced on the bridge as a benchmark for damage identification. It is shown that the proposed damage detection methodology is able to clearly indicate the presence of structural damage, if the damage leads to a change of the structural system (Dohler, Hille, Mevel, & Rucker, 2014).

Wipf et. al. proposed a structural health monitoring system by recording strain data under ambient traffic. The system was developed for the Iowa DOT bridge engineers to remotely and continuously monitor fracture critical bridges. The system provided detection of crack formation by identifying gradual changes in bridge structural behavior. A demonstration bridge was used to apply the structural health monitoring system. The application of the monitoring system to an existing bridge showed that the system could be used to monitor and detect damage (Wipf, Phares, Doornink, Greimann, & Wood, 2007).

1.3. Bridge Modeling

In order to monitor the structural health status of bridges still in use, the base line or health state is typically needed. In most cases, the base line data is provided through finite element modeling.

Much literature on bridge modeling has been published, which ranges from orthotropic plate theory, grillage theory, and full finite element modeling. The use of orthotropic plate theory to model beam-and-slab decks, typically in concrete bridges, has been quite common before the popular use of computers in structural analysis. Design curves of Rowe (Rowe, 1962)

and Cusens & Pama (Cusens & Pama, 1975) were used for bridge design several decades ago. However it is no longer considered an accurate method.

The grillage analogy is more accurate than the orthotropic plate theory for beam-and-slab decks. The grillage analogy involves the effective representation of a three- dimensional composite structure by a two- dimensional assemblage of discrete one- dimensional interconnected beams in bending and torsion. In analysis, the following assumptions need to be followed:

1. Concrete and steel are linearly elastic materials. The concrete slab is assumed to be able to sustain sufficient tension such that no tensile cracks develop in this part. The distribution of strains through the depth of each component is linear.
2. The longitudinal and transverse beams are assumed rigidly connected.

FEM modeling of bridges has long been researched, due to its versatile capability in capturing various geometry shapes and loading scenarios. For this reason it is often requested by clients, or proposed to a client, to perform such a most accurate analysis. Unfortunately, the method is cumbersome to use and is usually expensive. In addition, the choice of element type can be extremely critical and if incorrect, the results can be far more inaccurate than those predicted by simpler models such as grillage or orthotropic plates.

Grillage method is a widely used accurate method for bridge modeling, although the idealization of a bridge by a grillage is not axiomatic and is not without pitfalls. Jaeger and Bakht attempted to provide guidance on grillage idealization of various types of structure. Specifically, the principles on the idealization of slab, beam-and-slab, cellular, and voided-slab bridges were provided, with inclusion of idealization of slabs of linearly varying thickness and guidance on the mesh layout (Jaeger & Bakht, 1982).

Meng and Lui developed a refined stick model for preliminary dynamic analysis of skew bridges, which could be considered as a modified grillage method. The purpose of using the simplified stick modeling was to provide approximate results without developing a complex finite element model. Their modeling used a dual-beam stick representation of the bridge deck which was validated by comparing model's results with numerical solutions obtained for skew plates and a skew bridge. The authors found that the simplicity and ease of application of the method could be a valuable tool for preliminary analysis and seismic assessment of skew bridge response to dynamic loads (Meng & Lui, 2002).

Al-Saidy et al. used the grillage method to investigate the effect of damaged beam member on load distribution for their research on strengthening steel-concrete composite girders. The grillage method was selected for its simplicity and for the ability of any practicing engineer to understand its basic concepts (Al-Saidy, Klaiber, Wipf, Al-Jabri, & Al-Nuaimi, 2008).

Amer et al. used the grillage analogy to study various parameters affecting the equivalent width calculations of solid slab bridges used in the AASHTO LRFD bridge design codes. The authors used the grillage method because of its relative simplicity and reduced computational requirements. They also found the method provided sufficiently accurate results for simple single span bridges (Amer, Arockiasamy, & Shahawy, 1999).

Recently Lu and Shao performed a simplified analysis of a skew-plate bridge based on grillage analogy model. The structural behavior of a continuous reinforced concrete skew slab bridge was analyzed. The proposed grillage model has been validated by comparison with FEM results based on the shell model and the results obtained from field testing. In summary, grillage method has proven to be an accurate methodology to model bridges and has been adopted in practice, which could provide a good benchmark for the bridge health status (Lu & Shao, 2012).

1.4. Damage Index for Assessing Bridge Health Status

At present, bridges are generally rated and monitored during biennial inspections, largely using visual inspection techniques. There is the possibility that damage could go undetected at inspection or that growth of cracks in load-carrying members to critical levels, for instance, could occur between inspection intervals (e.g. see Gorlov, 1984). Sudden damage leading to bridge collapse also occurs due to collision, as evidenced by the AMTRAK railroad bridge collapse in the Southeastern US in 1993. The collapse was triggered by collision of the bridge pier with a barge. In order to facilitate the bridge health monitoring technique through non-visual inspection, a damage index needs to be developed, which will correlate with the damage existing in the structure. A damage index is typically calculated through displacement, strain, or acceleration measurements in a bridge, or uses the derivatives of these variables, such as slope and curvature.

Samali et al presented a research utilizing changes in modal strain energy between the undamaged and damaged states of plate-like structures for identifying damage in timber bridges, numerically and experimentally. A finite element model of the laboratory timber bridge was developed to investigate the capabilities and limitations of the method to detect damage. A simple four-girder bridge was fabricated and tested in a laboratory to verify the method. The numerical studies showed that the method can correctly identify single and multiple damage locations within the bridge. The experimental studies also showed promising results for detecting severe damage, but less effective for light and medium damage (Samali, Choi, & Crews, 2010).

Bonessio et al recently researched a procedure for the identification of the damage in bridge structures equipped with isolators and/or energy dissipating devices (Bonessio, Lomiento, & Benzoni, 2012). The procedure is based on the availability of accelerometric records from any

simple sensor network installed on existing bridges and compares changes in modal characteristics of the structural response. A new localization and severity index is introduced to be used for ordinary structural elements and anti-seismic devices. For this reason the procedure appears feasible for implementation on real structures with the advantage of providing direct indicators of the early stages of degradation of performance parameters. Although there is much literature on this topic, a suitable index depends on its sensitivity on bridge responses and the accuracy of measurement data.

1.5. Experimental Structural Health Monitoring Techniques Using Different Structural Response Variables

Static and dynamic testing of bridges has been performed for many years for a variety of different purposes. Early deflection and vibration measurements performed on fifteen bridges loaded by a constant load truck were summarized by Oehler. These tests were interrogated to identify the resonant frequencies of the bridge, measure their amplitude of vibration, and determine the susceptibility of these bridges to vibration (Oehler, 1957). The types of bridges tested include simple-span, continuous-span, and cantilever-type construction from either steel or reinforced concrete. Many practical observations regarding vibration response were presented. Further, an early summary of dynamic testing of highway bridges in the U.S. (simple, continuous and cantilever spans) performed between 1948 and 1965 was presented by Varney. The tabulation (without conclusions) was restricted to dynamic vehicular loading. Measured quantities were typically deflections and strains although a limited number of acceleration measurements were made (Varney, 1966).

Iwasaki, et al summarized tests performed in Japan to determine the dynamic properties of bridge structures. Excitation methods included eccentric mass shakers and, in one case, a

rocket engine. Resonant frequencies and damping ratios determined for individual piers and for the complete structures were summarized. Based on the results of 26 highway bridge tests performed between 1958 and 1969, an empirical relationship was established between the damping exhibited by the horizontal modes and the modal frequencies. Instrumentation of bridges for the purpose of measuring seismic response was reported along with a comparison of the response measured on one bridge during a forced vibration test and a subsequent seismic event (Iwasaki, Penzien, & Clough, 1972).

1.6. Thesis Overview

Although there has been much research done over the years, there are still issues with providing accurate and consistent monitoring techniques for bridge structures. In this thesis, an innovative modified curvature method is suggested to enhance bridge structural health monitoring efficiency. First, a numerical model of Cass County Bridge 32 is produced using the finite element modeling program, Abaqus. The model is benchmarked using field test data provided by Bridge Diagnostics, Inc. Next in Chapter 3 a damage localization method called Modified Curvature Method is proposed to accurately show damage introduced into the bridge model. Further verification of the proposed method is conducted in Chapter 4 with an in-lab experiment using a steel plate. Experimental modal analysis method is used to identify the mode shapes of the steel plate and the proposed Modified Curvature Method is applied to identify damage introduced to the steel plate. The thesis is completed in Chapter 5 with discussions on the conclusions of the work done in this thesis and possible future work needed to expand the topic of this thesis.

2. BENCHMARKED FINITE ELEMENT MODEL OF THE CASS COUNTY 32 BRIDGE

This chapter discusses the preliminary modeling results using the 'grillage method' of an incompletely documented bridge on Cass County Road 32. The bridge is located approximately 15 miles northwest of Fargo, ND. The 'grillage method' is a simple two dimensional model that idealizes the longitudinal and transverse stiffness of the deck and beams in a grid system. The bridge and finite element model will be discussed in more depth in the following sections.

2.1. Cass County Road 32 Bridge

2.1.1. Bridge Overview

The bridge is a single span beam-slab bridge with an overall length of 60 feet and a clear span of 57 feet. The superstructure is composed of 5 post-tension concrete I-beams and two intermediate diaphragms made of reinforced concrete. The deck is made of 6 inches of reinforced concrete with a small curb and steel railing along the edges. Figures 2.1 through 2.3 show in detail the dimensions of the bridge and the I-beams. Figures 2.1 through 2.3 show the bridge plan view, bridge cross-sectional dimensions, and the typical I-beam dimensions, respectively.

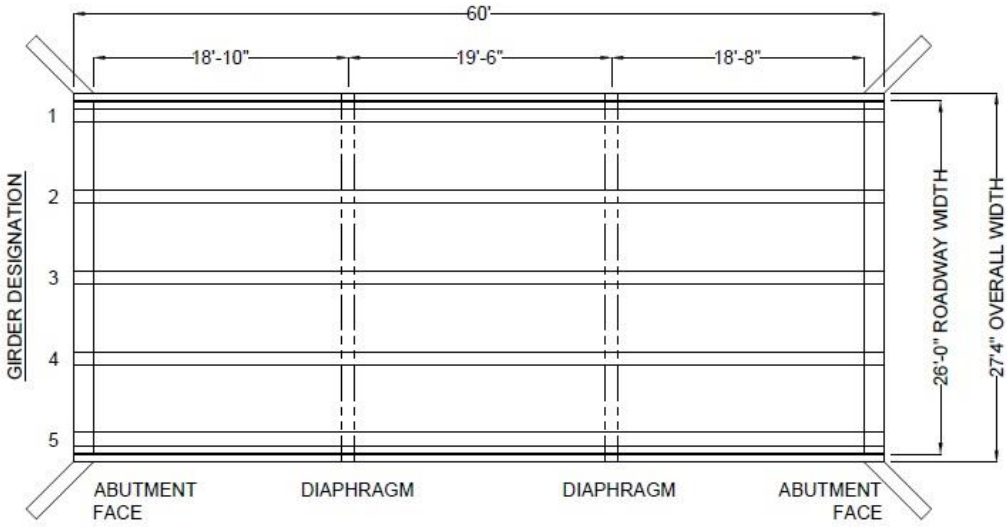

Figure 2.1. Plan view of Cass County Bridge 32

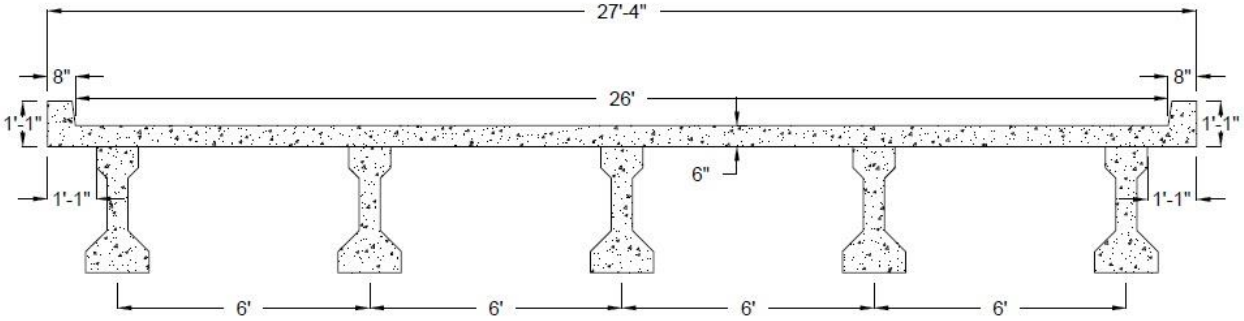

Figure 2.2. Cross-section of Cass County Bridge 32

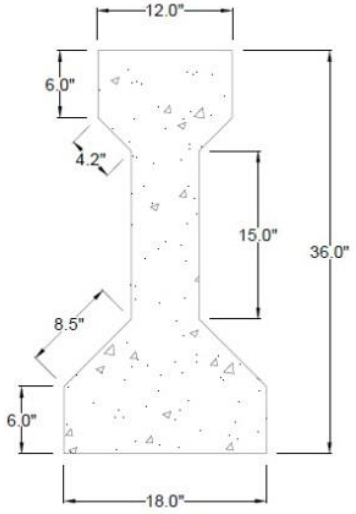

Figure 2.3. Typical bridge girder cross-section and dimensions

2.1.2. Bridge Diagnostics, Inc. (BDI) Load Testing

2.1.2.1. Sensors

The Cass County 32 Bridge was tested by Bridge Diagnostics, Inc. using a total of 39 sensors placed at three cross-sections of the bridge. Of the 39 sensors, there were 28 surface-mounted strain transducers, 5 cantilevered displacement sensors, and 6 tiltmeter rotation sensors. The displacement sensors were placed only at the cross-section B-B at midspan and the rotation sensors were placed at each end of beams 3 and 5. The strain sensors were placed on the bottom flange of all the post-tensioned beams at all three cross-section locations. For all the beams at midspan a strain sensor was placed on the top flange as well as at the end cross-sections of beams 3 and 5. Additionally, 4 strain sensors were placed on the top and bottom of the curb to monitor its response and determine if it was contributing structurally to the bridge. A detailed arrangement of the sensor deployment can be seen in Figure 2.4. Figure 2.5 shows the sensor layout at each of the three cross-sections. The sensors used for this load test are standard sensors typically used by BDI, which can be viewed in detail at their website (www.bridgetest.com).

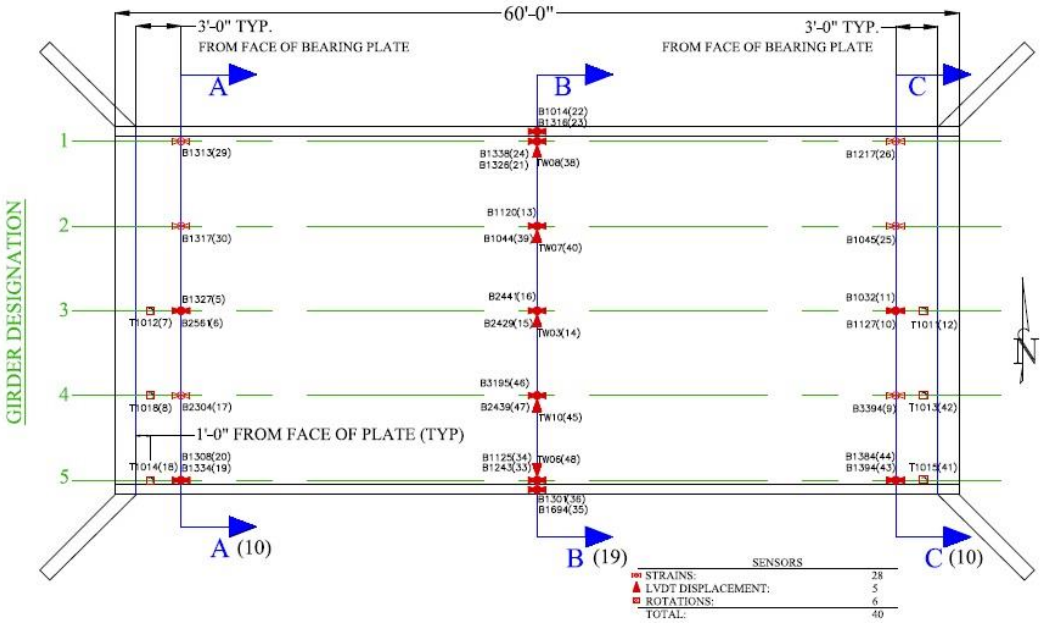

Figure 2.4. Sensor layout plan (Bridge Diagnostics, Inc., 2012)

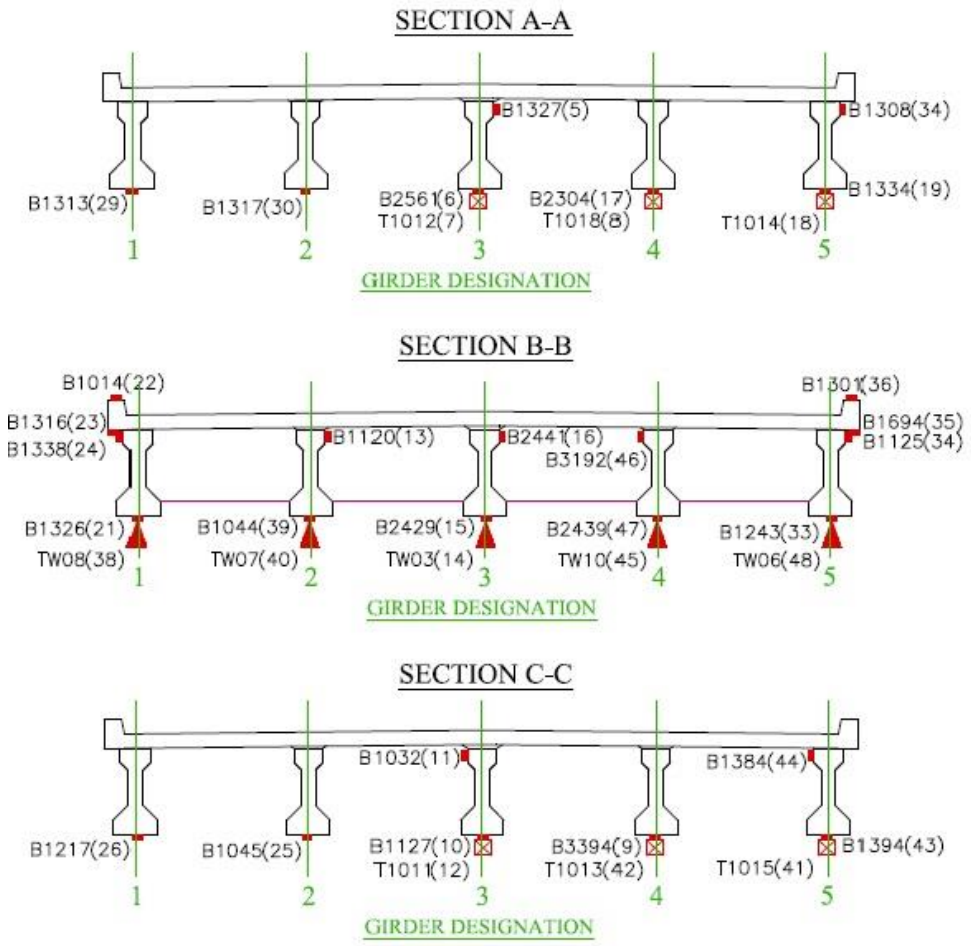

Figure 2.5. Cross-Section of sensor layout (Bridge Diagnostics, Inc., 2012)

2.1.2.2. Loading Procedure

To accurately measure the structural response of the bridge three different load paths were used, referred to as Path Y1, Y2 and Y3. The location of each load can be seen in Figures 2.6, 2.7, and 2.8 below. Cass County Public Works provided a standard dump truck loaded to 48 kips which traveled over the bridge at 3-5 mph. The rear wheel on the passenger side of the truck was equipped with a sensor to monitor the location of the truck with respect to time as it passed over the bridge. The truck location was recorded simultaneously with the data from the sensors attached to the bridge so the structural response data could be presented with respect to the truck location.

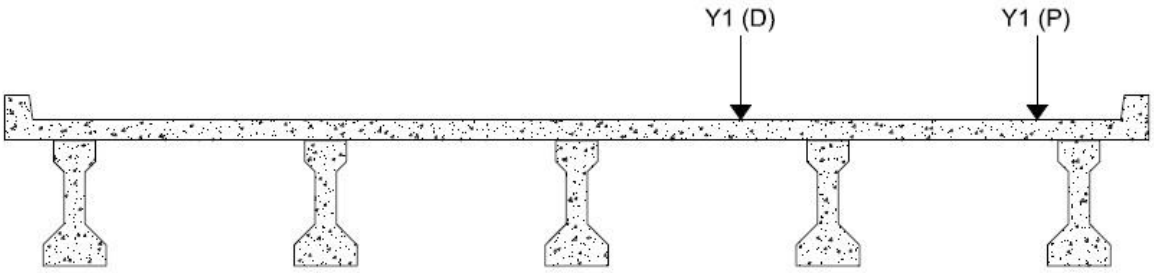

Figure 2.6. Truck path Y1

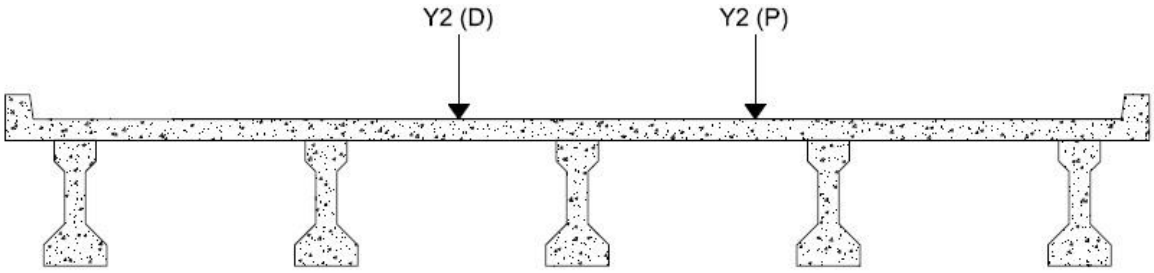

Figure 2.7. Truck path Y2

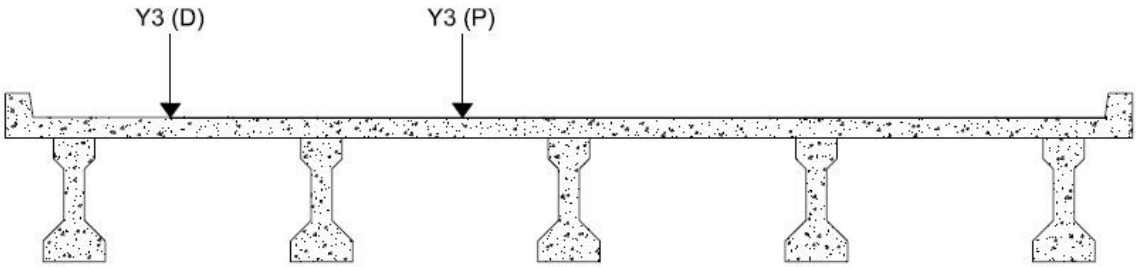

Figure 2.8. Truck path Y3

The truck passed over each load path twice to ensure a reliable data set was obtained for the analysis. In addition to passing over the bridge slowly one dynamic load test over Path Y2 was conducted at a speed of 35 mph to measure dynamic load effect.

2.1.2.3. Load Test Data and Results

After recording the raw data from the sensors BDI processed the data using their own software program. The results were then evaluated by their engineers to ensure the data was of good quality. This was shown by having the strain measurements return to zero after loading and

good reproducibility of responses. The strain measurements returning to zero after loading is also a good indication of elastic behavior of the beam. BDI also investigated the neutral axis depth from the strain measurements and the depth was found to be fairly consistent throughout each beam. This is also an indicator of elastic behavior, which makes modeling of the bridge a less complicated task. Figure 2.9 below shows the strain results from three sensors for the two tests of each load path. Similarly, Figure 2.10 shows the deflection results.

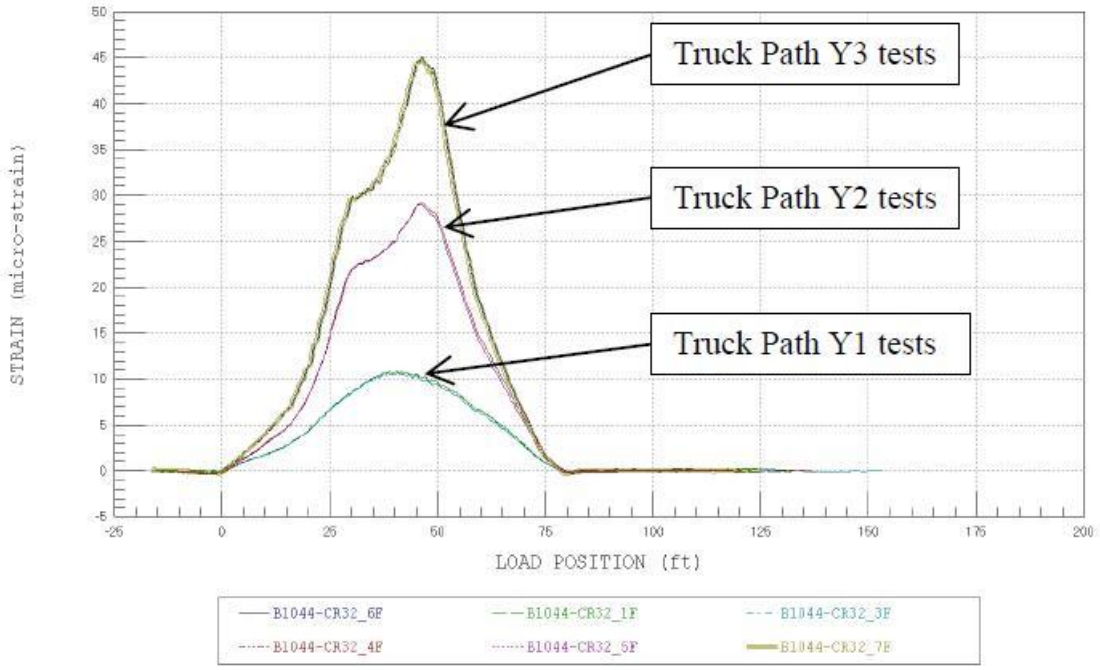

Figure 2.9. Strain reproducibility (Bridge Diagnostics, Inc., 2012)

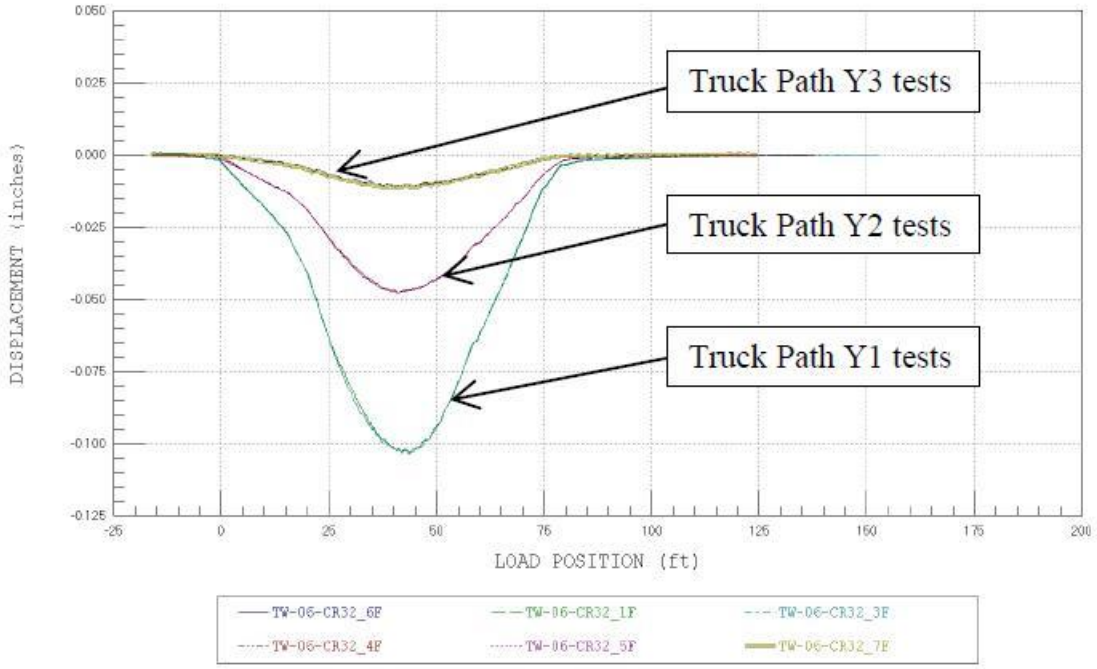

Figure 2.10. Deflection reproducibility (Bridge Diagnostics, Inc., 2012)

A typical strain response of the bottom flange at midspan can be seen in Figure 2.11. The figure shows the recorded strain responses of the bridge under the Y1 load path. As expected, beam 5 experienced the largest strain responses from the truck load and the level of strain decreased from beam 4 to beam 1. Since beams 1 and 2 experienced noticeable strain response, one can see that the diaphragms and deck at some level transfer the load laterally. The maximum strain occurs when the truck's front axle is approximately 45.0 feet from the beginning of the bridge. This is also the case when the truck's second axle is approximately located at the midspan of the bridge. The positive strain values show that the bottom flange is in tension.

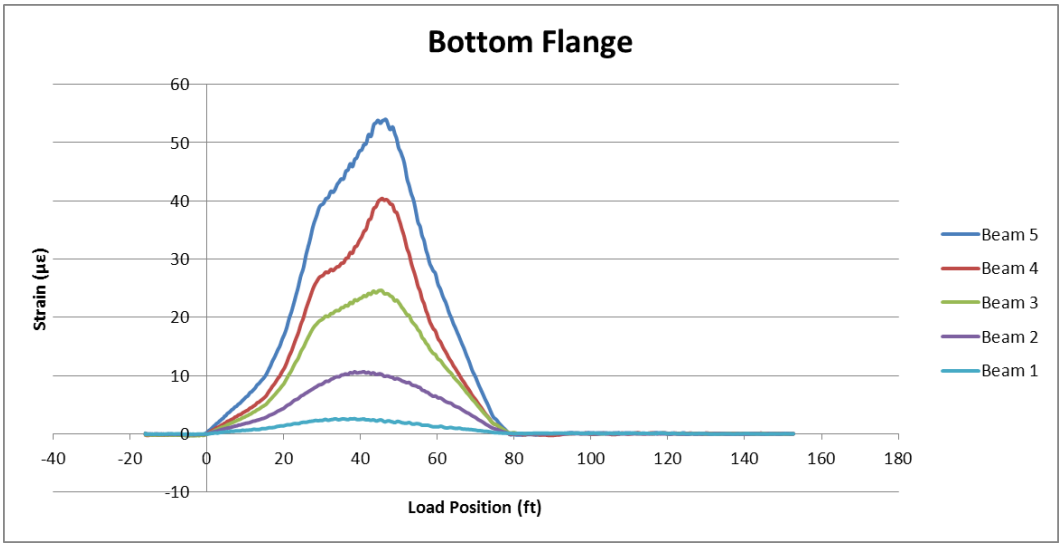

Figure 2.11. Midspan bottom flange strain response from load path Y1

Figure 2.12 below shows a typical strain response of the top flange of the beams at midspan. Like the responses of the bottom flange, the largest response is seen at beam 5 with decreasing magnitude from beam 4 to beam 1. The localized spikes in strain that can be predominately seen in the beam 5 data and to a lesser extent in the beam 3 and 4 data, this is the result of the truck axle passing directly over the strain sensor location.

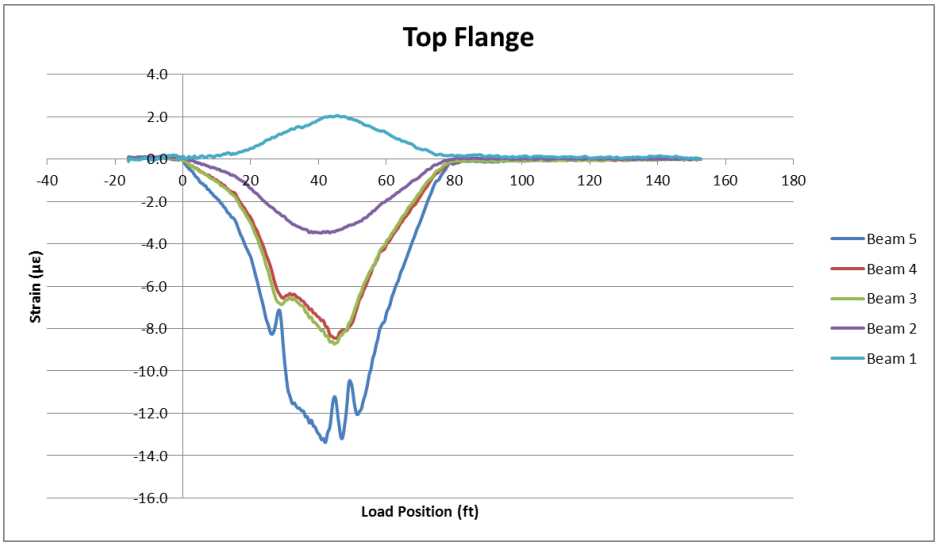

Figure 2.12. Midspan top flange strain response from load path Y1

Figure 2.13 shows the strain comparison of the top and bottom flange of beam 5. It can be seen that the top flange is in compression and the bottom flange is in tension. The large

difference in magnitude between the two flanges and the similar shape of the response shows that the deck and beams are in composite action. The fact that the top flange experiences such smaller compression strains compared to the bottom flange tension strain indicates that deck slab is experiencing most of the compression strain.

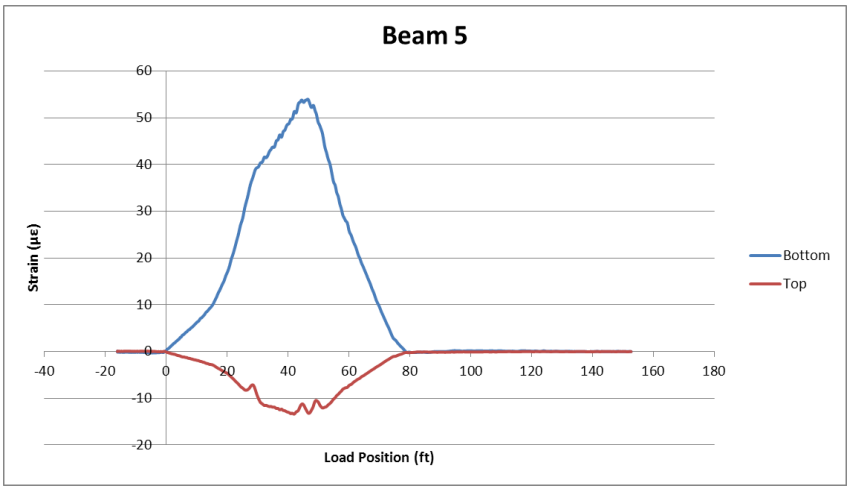

Figure 2.13. Observed composite behavior

Figure 2.14 below shows the measured displacement at midspan of beams 1 through 5. The displacement measurements for all beams return to zero after loading which indicates elastic behavior for the whole structural system. As expected, the greatest displacement observed was at beams 4 and 5 which are the closest beams to load path Y1. Also the maximum displacement occurs when the truck's front axle is located approximately 42.0 feet from the start of the bridge. At that location the second axle is passing over the midspan of the bridge, the resultant force from the truck load is at this location.

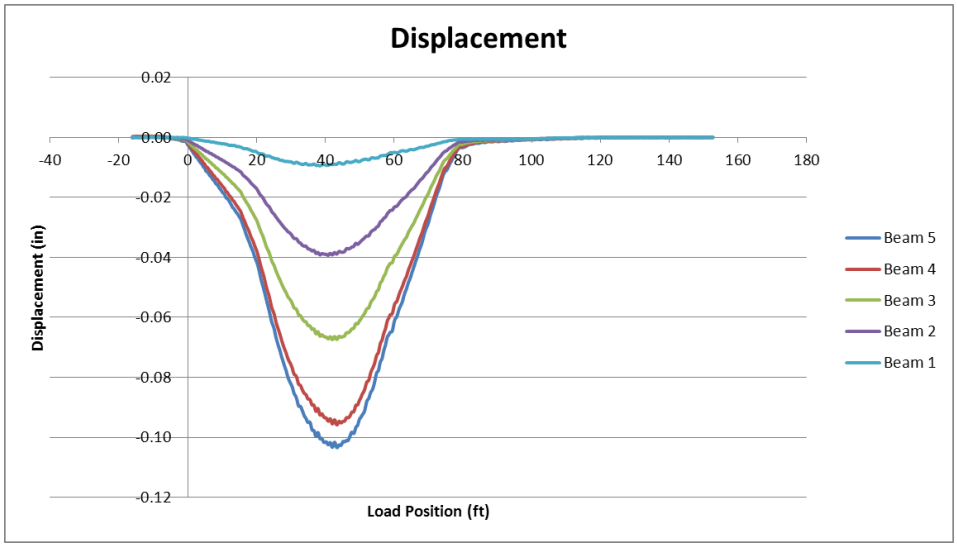

Figure 2.14. Measured midspan displacement from load path Y1

With the load test data provided by BDI, Inc. a series of analytical models can be developed to investigate the bridge structure. With an accurate model, simulations of a compromised structure can be developed and analyzed to show the reliability of this structure with varying levels of damage.

2.2. Benchmarked Finite Element Model of Cass County 32 Bridge

2.2.1. Model Development

The developed model was verified using field data obtain from Bridge Diagnostics, Inc. (BDI) who was hired by the Cass County Highway Department to investigate the structural integrity of this bridge and another bridge on Cass County Road 4. Based on the field test results, a modified curvature based bridge health monitoring methodology is suggested, which could relate the deformation measurements at several locations of the bridge with the structural health status of the bridge, or directly with the ratings of the bridge.

2.2.1.1. Grillage Method

Background

The Grillage method is a simple modeling method used to represent the stiffness of the deck through longitudinal and transverse beams. This method is commonly used among state DOTs to quickly analyze a simple beam-slab bridge structure. Typically the longitudinal beams are placed where the actual bridge girders are located and also depend on the width of the bridge deck. The stiffness of these beams and the effective width of the deck are combined together to determine an approximate effective stiffness. Transverse members are placed at about 1.5 times the spacing of the longitudinal members. It is recommended that the spacing ratio not exceed 2:1. Transverse members should also be placed where any diaphragms are located. The stiffness of the transverse members is the transverse stiffness of the bridge deck. At locations where there is a diaphragm, the stiffness of both the deck and the diaphragm should be calculated (Jaeger and Bakht, 1982).

Model Development

The finite element program Abaqus was used to develop the grillage model. Five longitudinal beams were used to idealize the longitudinal stiffness of the bridge. The locations of these beams are where the actual bridge girders are located, which are spaced at 72.0 inches on center. Five transverse beams were used to idealize the transverse stiffness of the bridge and two of which are placed at the diaphragms. The transverse beams were spaced at 117.0 inches on center. The end boundary conditions were initially set as completely fixed, this was determined from visual observation of the beams end conditions at the site. The end of the bridge girders were set on the abutments and had been fully grouted. After running the model through analysis the results showed issues with the magnitude of the deflection compared to the actual field

measurements, which were more than 50% less in some cases. It was determined that end boundary conditions needed to be relaxed in order to mitigate the problem. An axial spring and a rotational spring were added at each end of the beams. The results from the model were more agreeable with the field data after this change. Figure 2.15 below shows the basic layout of the bridge model.

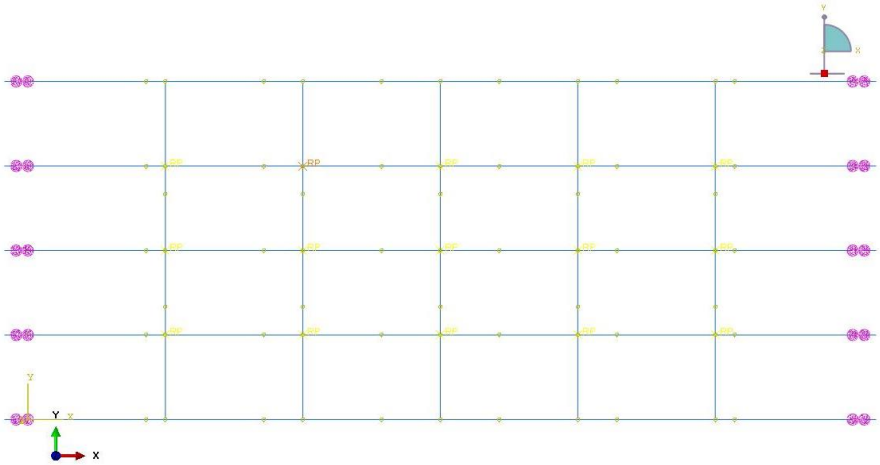

Figure 2.15. Finite element bridge model

The calculations for idealized stiffness of both the longitudinal and transverse members were completed using an effective stiffness equation which took into consideration the contribution of the reinforcing steel. The Young's modulus for the deck concrete and beam concrete was calculated using Eq. 2.1 and f_c' = 4500 psi and 5500 psi for the deck and beam respectively. The concrete strength of the bridge deck and girders were taken from BDI's final report on the bridge and represents an effective value of the field concrete strength through non-destructive testing.

$$E_C = 57000\sqrt{f_c'} \qquad \text{Eq. 2.1}$$

With the Young's Modulus of the beam and deck, the combined modulus was calculated using Eq. 2.2. Based on the BDI's Ground Penetrating Radar (GPR) inspection of the deck, it

was found that the reinforcement spacing for the top and bottom of the deck in the longitudinal direction was 16.0 inches and 12.0 inches, respectively. For the transverse direction both the top and bottom reinforcement spacing was found to be 12.0 inches. It was assumed that #4 bar was used for the reinforcement. For the post-tensioned beams there are three ducts for the post-tension wires which each mostly likely hold 22, 0.25" wires. There are also two reinforcement bars set in the top flange of the post-tensioned beams, for the calculation these were assumed to be #6 bar.

For longitudinal members,

$$E_{rc} = E_{c,eff} * \left(1 + \frac{(A_{st,deck} + A_{st,beam}) * \frac{E_S}{E_C}}{A}\right) \quad \text{Eq. 2.2}$$

$$E_{c,eff} = \frac{(E_{beam} * A_{beam}) + (E_{deck} * A_{deck})}{A} \quad \text{Eq. 2.3}$$

For transverse members,

$$E_{rc} = E_c \left(1 + \frac{A_{st,deck} * \frac{E_S}{E_C}}{A}\right) \quad \text{Eq. 2.4}$$

At diaphragm,

$$E_{rc} = E_c \left(1 + \frac{(A_{st,deck} + A_{st,diaph}) * \frac{E_S}{E_C}}{A}\right) \quad \text{Eq. 2.5}$$

E_{rc} is the Young's Modulus of all the components combined together, including the concrete and reinforcing steel.

During the modeling process it was required to define a section for the longitudinal and transverse members. When defining the beam section, the parameter of the neutral axis is required. The longitudinal members being a composite section of the beam and deck, the strain measurements from the field test data could be used to estimate the actual neutral axis depth. The following equation was used to determine the neutral axis depth at each data point.

$$E_{rc} = 36" + \left(\varepsilon_{tf} + \frac{36"}{\varepsilon_{bf}+\varepsilon_{tf}}\right) \quad \text{Eq. 2.6}$$

Considering the beams are 36.0” deep and the deck has a thickness of 6.0”, only the data points that produced a value in the range of 15.0” to 36.0” were considered further. The values in the specified range were then averaged for each beam under different load paths. The values were further averaged combining those values at the three cross-sections and load paths. An overall average value for an interior beam and exterior beam was finally calculated. A value of 26.2” and 27.1” was determined for the interior beams and exterior beams, respectively. The neutral axis values are measured from the bottom of the beam. These values are reasonable considering the beams and deck act as a composite section. For comparison purposes the neutral axis depth was calculated by hand for a typical interior beam and exterior beam. The calculated value for the interior beam and exterior beam were 28.3” and 26.8”, respectively. This comparison shows that there is composite action between the beam and deck and also the values produced from the field data are reasonable.

Initially the model’s end support conditions were fully fixed because of reasons discussed earlier. After analysis and adjusting parameters of the beams it was found that changing the end conditions by adding an axial and rotational spring at each end of the longitudinal members worked well. This allowed the beams to translate longitudinally and rotate about the transverse axis. The stiffness values of the springs were adjusted individually until the best possible match with the field results was obtained. After the adjustment, displacement values from the model matched well with the field data in several locations under different loading paths. The stiffness values for each spring are shown in Table 2.1.

Table 2.1. Stiffness values for springs

Location	Axial Spring, West (kip/in)	Axial Spring, East, (kip/in)	Rotational Springs, (kip/in)
Beam1	1	1	1
Beam 2	1020	528	480
Beam 3	762	398	362
Beam 4	1116	578	525
Beam 5	2125	1100	1000

To simulate the truck moving across the bridge, concentrated point loads were applied where the wheels were located and moved in 3 foot increments. Using linear approximation, the effective point load was determined where each longitudinal and transverse element intersect. Figure 2.16 below represents one section of the model grid and Eq. 2.7 through 2.12 show the methodology used. The wheel load, P, is the actual location of the truck tire. P_1 and P_2 are the linearly distributed loads from P to the transverse members, which are then linearly distributed again to the four corners. The moment induced in the longitudinal direction by transferring the wheel load to the transverse members (P_1 and P_2) was neglected in the analysis because the error created is small and can be ignored. The moment induced in the transverse direction by transferring P_1 and P_2 to the four nodes was also ignored because there is no cantilever type loading in the model and most of the wheel lines are less than 2 feet from the nearest longitudinal member. For these reasons the error in both the longitudinal and transverse directions should be negligible (Jaeger and Bakht, 1982).

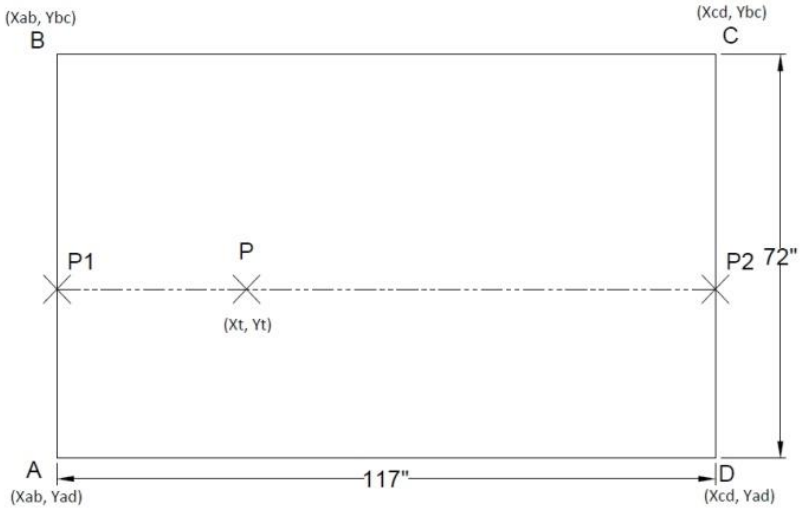

Figure 2.16. Load distribution to member intersections

$$P_1 = P\frac{X_t - X_{ab}}{117"} \quad \text{Eq. 2.7}$$

$$P_2 = P\frac{X_{cd} - X_t}{117"} \quad \text{Eq. 2.8}$$

$$P_A = P_1\frac{Y_{bc} - Y_t}{72"} \quad \text{Eq. 2.9}$$

$$P_B = P_1\frac{Y_t - Y_{ad}}{72"} \quad \text{Eq. 2.10}$$

$$P_C = P_2\frac{Y_t - Y_{ad}}{72"} \quad \text{Eq. 2.11}$$

$$P_D = P_2\frac{Y_{bc} - Y_t}{72"} \quad \text{Eq. 2.12}$$

P_A, P_B, P_C, and P_D are the effective loads at points A, B, C, and D, respectively. The following figure shows the trucks footprint (Figure 2.17). The dual wheels for axles 2 and 3 were applied as one point load in the model.

Figure 2.17. Test truck footprint

A mesh sensitivity analysis was conducted to confirm accuracy of the model results. For this analysis the peak deflection results at the midspan of Beam 3 were used. Mesh length was adjusted starting with a length of 100 inches and was reduced to 50 inches, 30 inches, 20 inches, and finally 10 inches. At a mesh length of 10 inches it was determined that the model results had sufficiently converged to an accurate result. Figure 2.18 graphically shows the mesh sensitivity analysis is complete.

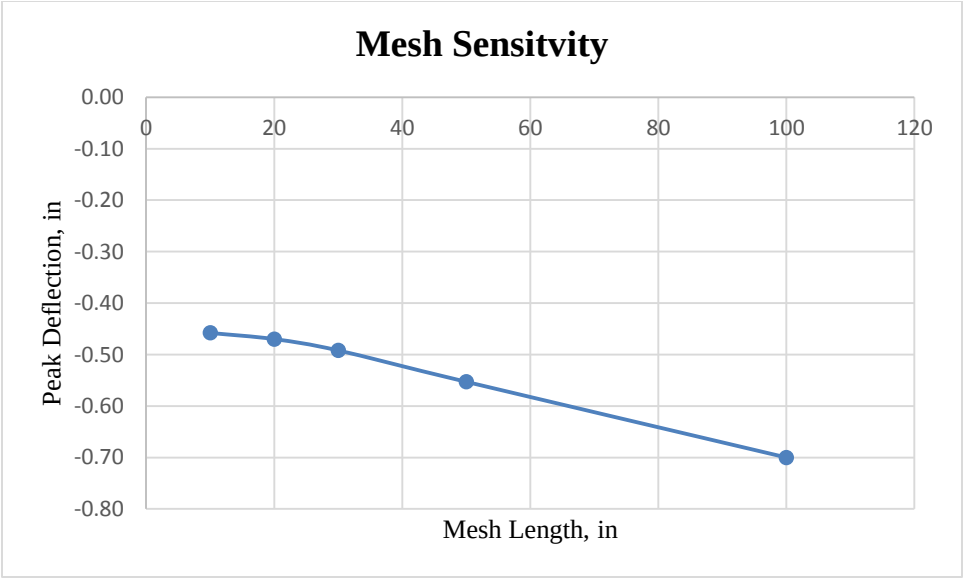

Figure 2.18. Mesh sensitivity analysis

2.2.2. Model Results

The model results obtained were directly compared to the deflection measurements collected by BDI, Inc. After several simulation trials adjusting the axial and rotational spring stiffness, a model was obtained where several locations under different load paths had a good matching with the actual deflection measurements, although, there were some parts of the model which did not match the field results. It was determined that this model could be used further for damage analysis and the initial development of a damage index. The Figure 2.20 through 2.25 show where the model was able to match the field measurement well. Figure 2.19 shows the bridge's position relative to the load position shown in Figures 2.20 through 2.25.

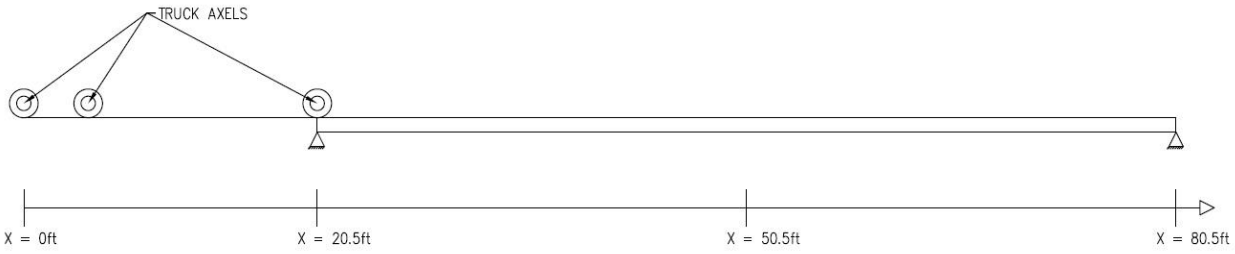

Figure 2.19. Relative bridge position

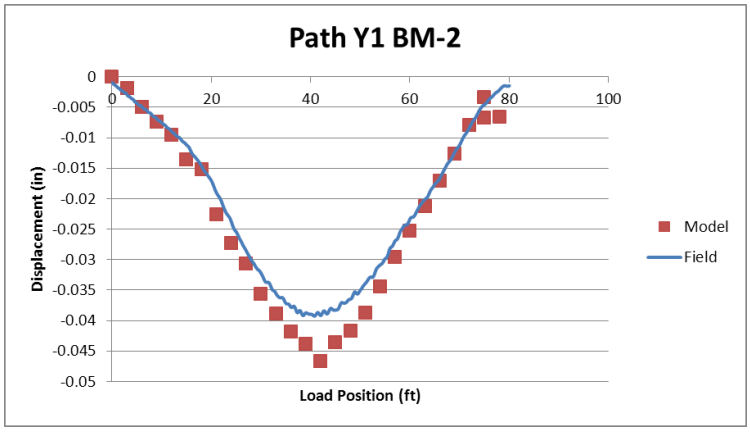

Figure 2.20. Model and measured data comparison: load path Y1 and beam 2

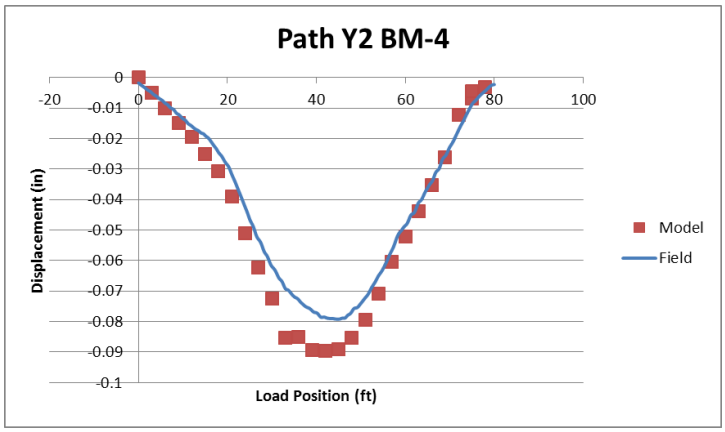

Figure 2.21. Model and measured data comparison: load path Y2 and beam 4

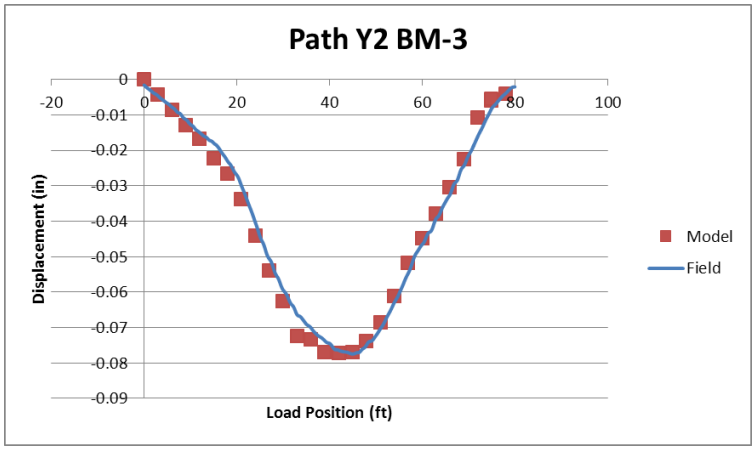

Figure 2.22. Model and measured data comparison: load path Y2 and beam 3

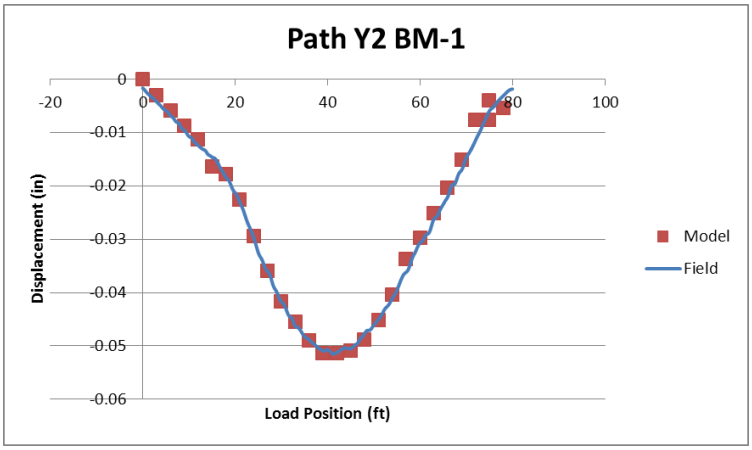

Figure 2.23. Model and measured data comparison: load path Y2 and beam 1

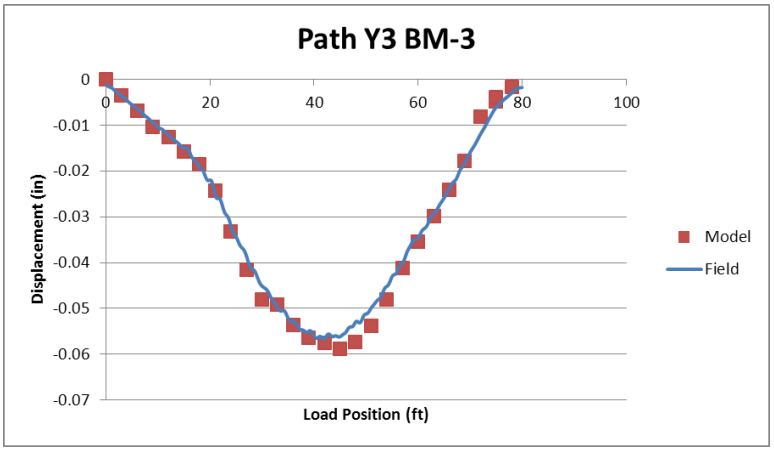

Figure 2.24. Model and field data comparison: load path Y3 and beam 3

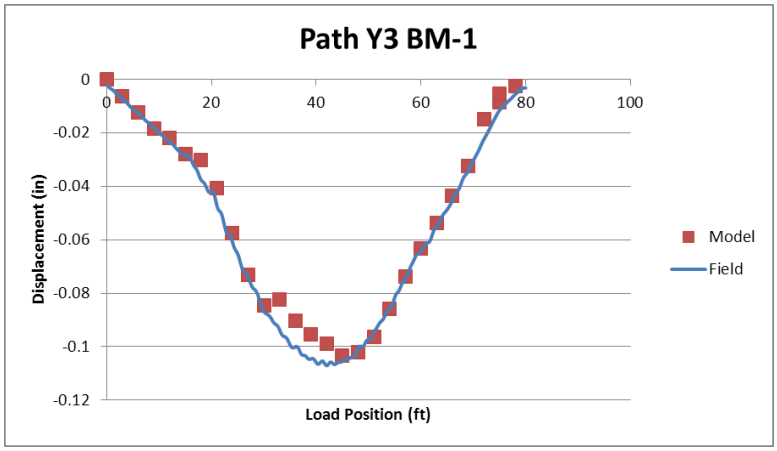

Figure 2.25. Model and field data comparison: load path Y3 and beam 1

2.2.3. Data Summary

In the results shown above it can be seen that the developed model produces accurate results when compared to the field data. For example Figure 2.23 shows the model data follows the field data almost exactly. In Figure 2.21 there is some discrepancy when comparing the field and model data. The model data shows a higher peak deflection than that in the field, but the magnitude of the deflection difference is approximately one hundredth of an inch. When considering the total length of the bridge this difference in deflection is negligible. In these figures the rate of deflection in field and in the numerical model still matches very well. Based

on Figures 2.20 - 2.25, it is concluded that the developed finite element model accurately represents the behavior of the bridge tested in the field.

2.3. Summary and Conclusions

This chapter outlined the steps used in the development of the numerical model as well as adjustments in the model made to match the field data. Using the Grillage Method is a simple and accurate way to represent conventional beam slab bridges which are very common throughout the U.S. It has been concluded that the numerical model accurately represents the tested bridge. This representative model can be further adopted to verify the proposed damage detection methodology. Investigation of the proposed damage detection method using the developed model is described in Chapter 3.

3. DAMAGE LOCALIZATION THROUGH THE MODIFIED CURVATURE METHOD

In this section a modified curvature method used in damage localization is described. The curvature method uses modal deflection data from a numerical model. With the modal deflection data curvature in the longitudinal, transverse, and torsional directions are calculated and combined to create composite curvature of the bridge. The highest change of the composite curvature is represented in three-dimensional contour plots through MATLAB, which indicates the most possible damage location.

3.1. Methodology

Based on the finite element modal deflection data, the modified curvature method was used to obtain the plots shown in this thesis.

3.1.1. FEA Modal Analysis and Data

Using the FEA model described in the previous chapter, modal deflection data for the first five modes are used. After obtaining the modal data from the undamaged state of the FEA model, five damage cases are simulated to test the damage localization capability of the modified curvature method. Figure 3.1 shows the location of each damage case in red. To simulate damage in the bridge, a 75% reduction in stiffness was applied in each damage case. The large stiffness reduction is used to indicate the severity of the damage.

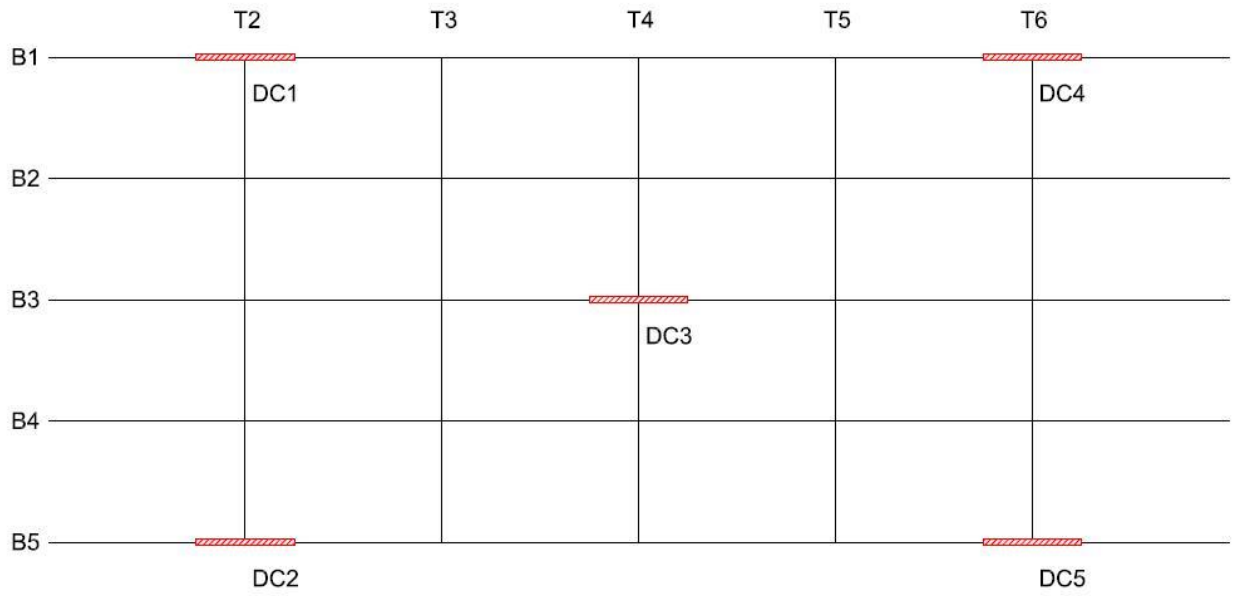

Figure 3.1. Location of damage cases (DC)

The reduced stiffness was applied to beam 1, 3, and 5 at different locations along the length of each beam. The longitudinal location and length of damage is detailed in Table 3.1. The center of each of these sections is located at a transverse member of the model (T2, T4, and T6). Each simulation was completed with one section of the beams having the 75% reduced stiffness.

Table 3.1. Longitudinal location and length of damage

Section	Length of Section	Distance between center of section and center of left bearing
1	4'10'	9'9"
2	9'9"	29'3"
3	9'9"	48'9"

Modal analysis was conducted for each of the five damage cases to obtain the modal deflection data. The first five modes were analyzed. The deflection data from each mode shape

was then organized in Microsoft Excel spreadsheet. With the modal deflection data, the curvature was calculated in the longitudinal, transverse, and torsional directions.

The curvature in the transverse direction was calculated using Equation 3.1. Curvature in the longitudinal direction was calculated using Equation 3.2. For the point locations on the edge members, the term associated with point outside the domain of the model is taken as zero when they are at the free edge of the bridge, while the term associated with point outside the domain of the model along the fixed edge is taken as equal to the displacement of the edge point.

Transverse direction,

$$K_{ij} = \frac{2u_{ij} - u_{(i+1)j} - u_{(i-1)j}}{\Delta H^2} \quad \text{Eq. 3.1}$$

Longitudinal direction,

$$K_{ij} = \frac{2u_{ij} - u_{i(j+1)} - u_{i(j-1)}}{\Delta L^2} \quad \text{Eq. 3.2}$$

i represents the beam identification (1, 2, 3, 4, or 5) and j represents the transverse member (2, 3, 4, 5, or 6). K_{ij} is the curvature at its respective location and u_{ij} is the deflection produced from the model. ΔH is the distance between the two point locations in the transverse direction of the bridge, for this model that distance is 72.0 in. ΔL represents the distance between two points in the longitudinal direction of the bridge, this value is 117.0 in.

The determination of the torsional component of the modified curvature method is completed by using Eq. 3.3. to find the torsional curvature of the bridge model located in the space between the intersections of the beams and transverse members. The *k* corresponds to each of the 16 blocks formed by the beams and the girders of the bridge. In order to obtain a torsional curvature component of the modified curvature method, a value must be obtained for each *ij* location. This is simply obtained by taking an average of all the K_k values in which the *ij* location is the corner of the spaces. For example, the torsional curvature at the intersection of B2

and T4 would be the average of K_2, K_3, K_6, and K_7. The torsional curvature for the intersection of B5 and T3 would be the average of K_{13} and K_{14}. Finally, for torsional curvature at the intersection of B1 and T2 would simply be K_1.

The torsional curvature is defined as:

$$K_k = \frac{\frac{u_{(i+1)j} - u_{ij}}{\Delta H} - \frac{u_{(i+1)(j+1)} - u_{i(j+1)}}{\Delta H}}{\Delta L} \quad \text{Eq. 3.3}$$

With the curvature components for longitudinal, transverse, and torsion obtained for the undamaged state and the all damaged cases, they are combined into Eq. 3.4 to represent the overall change in curvature at each point.

$$K'_{ij} = \sqrt{K_{Tr}^2 + K_L^2 + K_{To}^2} - \sqrt{K_{Tr,h}^2 + K_{L,h}^2 + K_{To,h}^2} \quad \text{Eq. 3.4}$$

Where K_{Tr}, K_L, K_{To} are the transverse, longitudinal, and torsional curvatures for the damaged bridge; $K_{Tr,h}$, $K_{L,h}$, $K_{To,h}$ are the transverse, longitudinal, and torsional curvatures for the health bridge.

3.1.2. Results and Discussion

The following plots show the change in curvature for each of the five damage cases. The results show a good correlation between the increased change in curvature and the damage location.

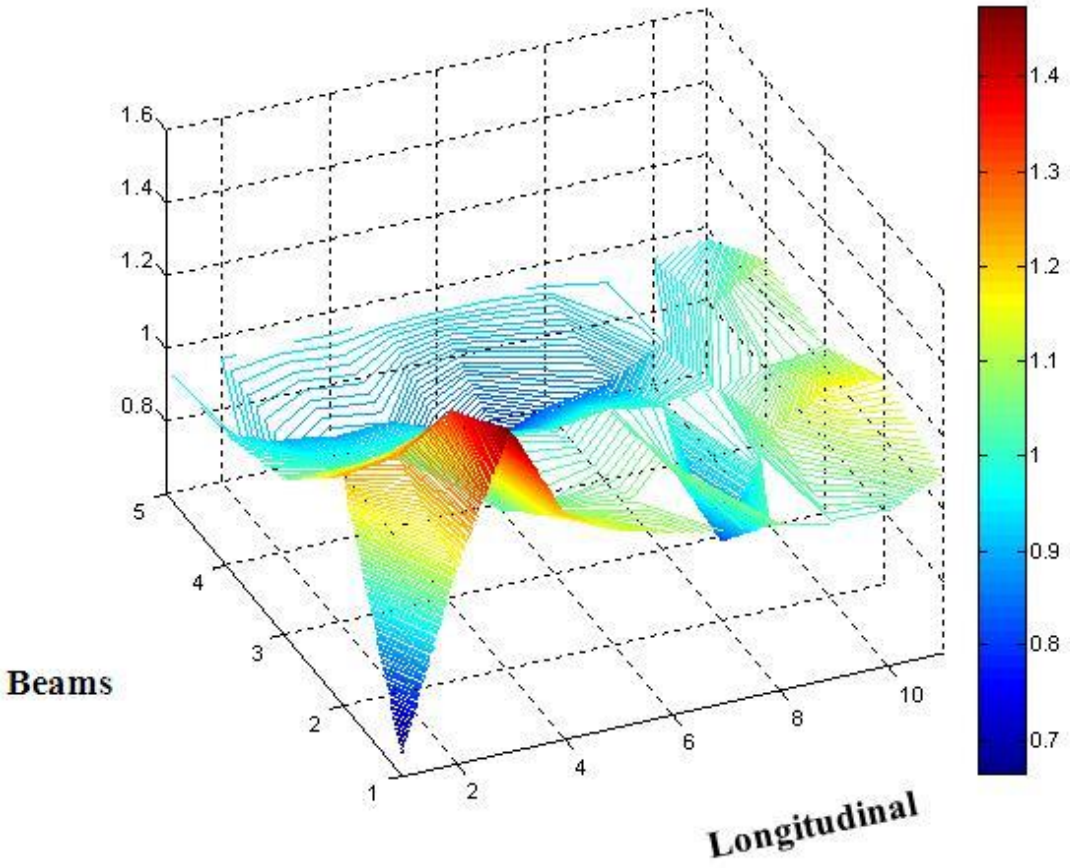

Figure 3.2. Change in model curvature: damage case 1

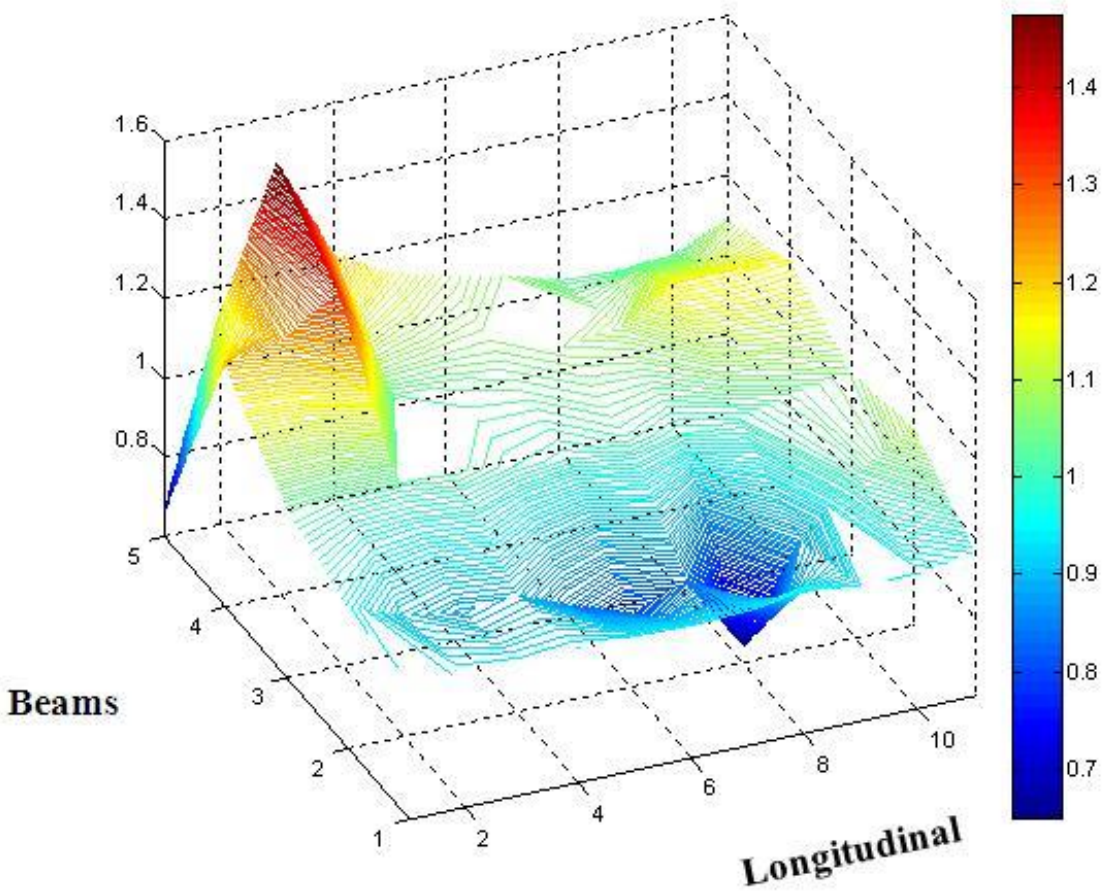

Figure 3.3. Change in model curvature: damage case 2

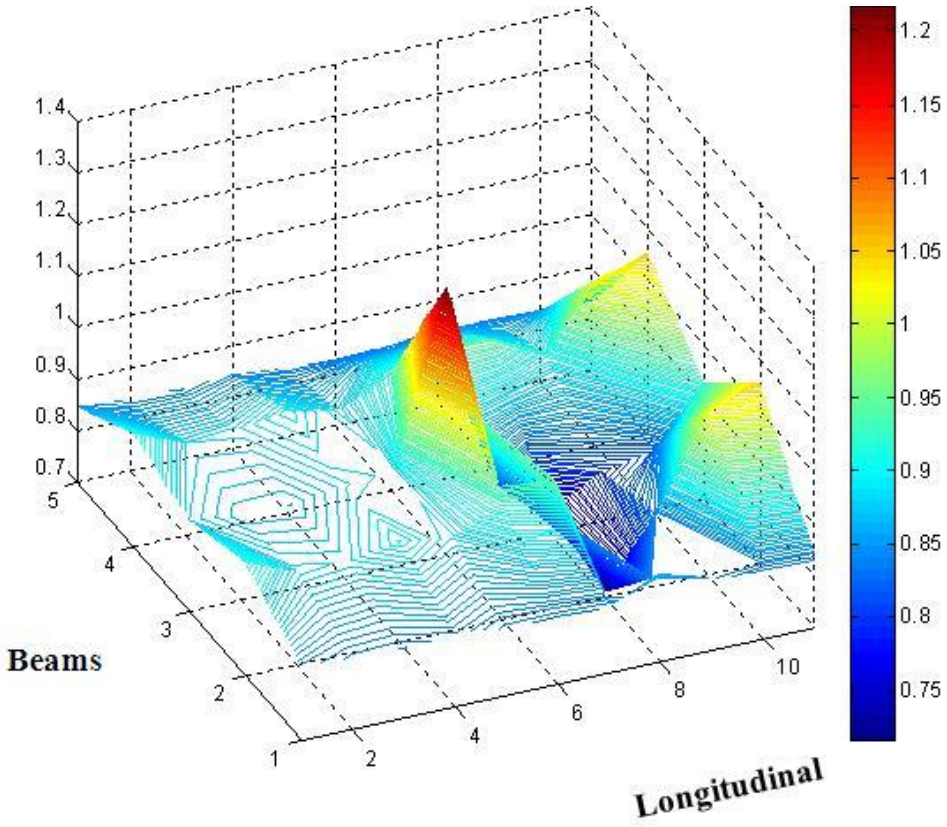

Figure 3.4. Change in model curvature: damage case 3

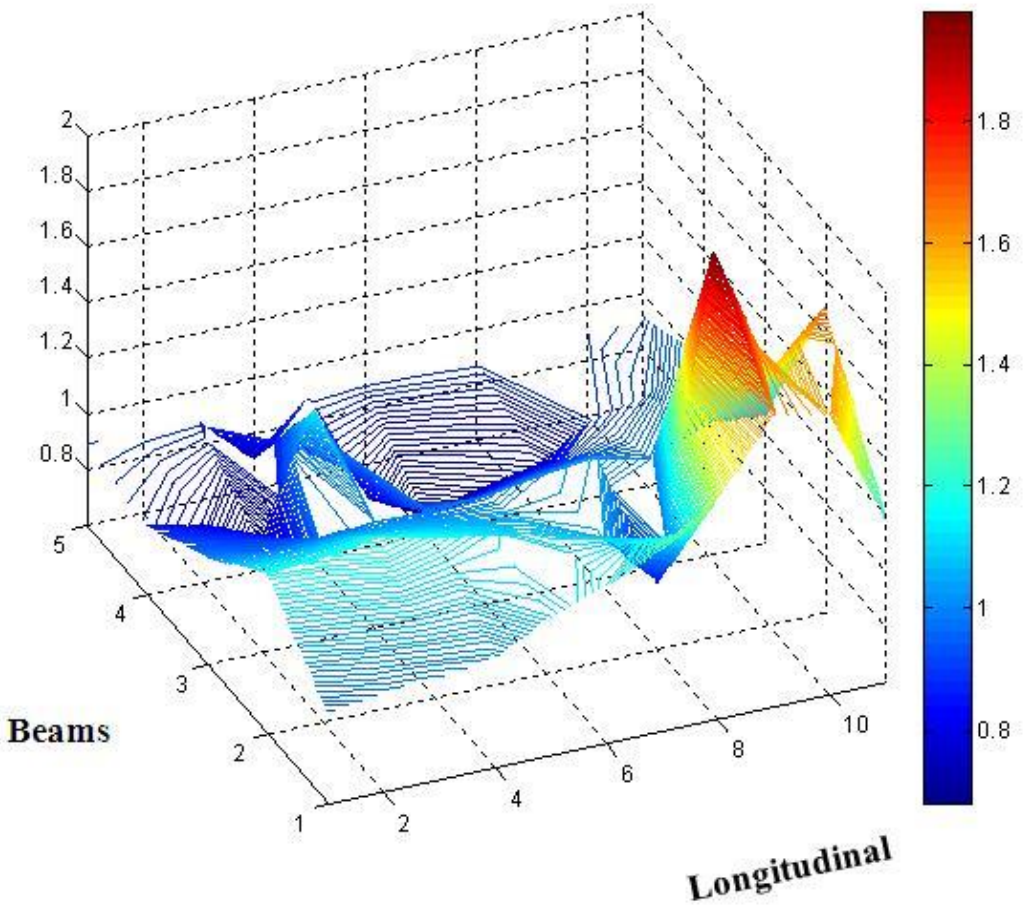

Figure 3.5. Change in model curvature: damage case 4

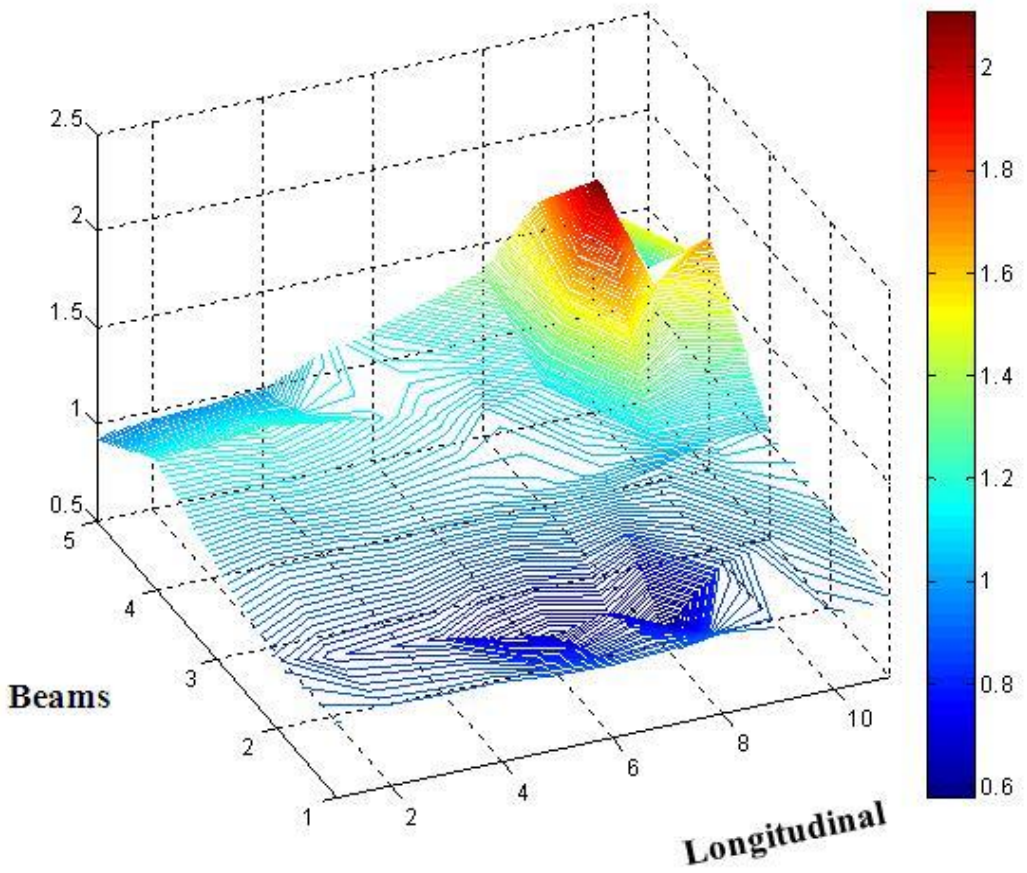

Figure 3.6. Change in model curvature: damage case 5

As seen in Figures 3.2 to 3.6, the modified curvature equation locates the damaged area well. The contour graph of the change in curvature shows an obvious peak where the damage is located on the bridge. Although there are some minor peaks in the contours at other locations the highest peak clearly shows the actual damage location. The other peaks may be due to data noise from the model. Based on the results from Figure3 3.2 to 3.6, it can be clearly seen that the modified curvature method can accurately locate damage by combining the curvature calculations in the longitudinal and transverse directions as well as the torsional curvature.

3.2. Comparison with Literature Results

3.2.1. Previously Developed Damage Index Method

The damage index method developed by Stubbs and Kim was used to locate damage in structures with the availability of the characteristic mode shapes before and after damage. Equation 3.5 is the damage index they developed. A damage index, β, is used for structures that can be represented as a beam. This damage index is developed based on the change in strain energy stored in the structure when it deforms in its particular mode shape. For a damage index at location *j* on the beam for the *i*th mode strain energy the following equation is used,

$$\beta = \frac{(\int_a^b [\psi_i^{*"}(x)]^2 dx + \int_0^L [\psi_i^{*"}(x)]^2 dx)}{(\int_a^b [\psi_i^{"}(x)]^2 dx + \int_0^L [\psi_i^{"}(x)]^2 dx)} \frac{\int_0^L [\psi_i^{"}(x)]^2 dx}{\int_0^L [\psi_i^{*"}(x)]^2} \quad \text{Eq. 3.5}$$

Where *L* is the length of the beam, *a* and *b* are the limits of a segment of the beam where damage is being analyzed. $\psi_i^{"}(x)$ and $\psi_i^{*"}(x)$ are the second derivatives of the *i*th mode shape corresponding to the undamaged and damaged structures, respectively (Kim & Stubbs, 1995).

In an effort to further validate the proposed modified curvature method a direct comparison with the damage index method suggested by Stubbs and Kim was completed. In this comparison the bridge model was evaluated with the damage index method in its undamaged state as well as the five damaged cases. The two methods were directly compared using the three dimensional contour plots created in MATLAB. Figures 3.7 through 3.11 show the results of the Damage Index Method for damage cases one through five.

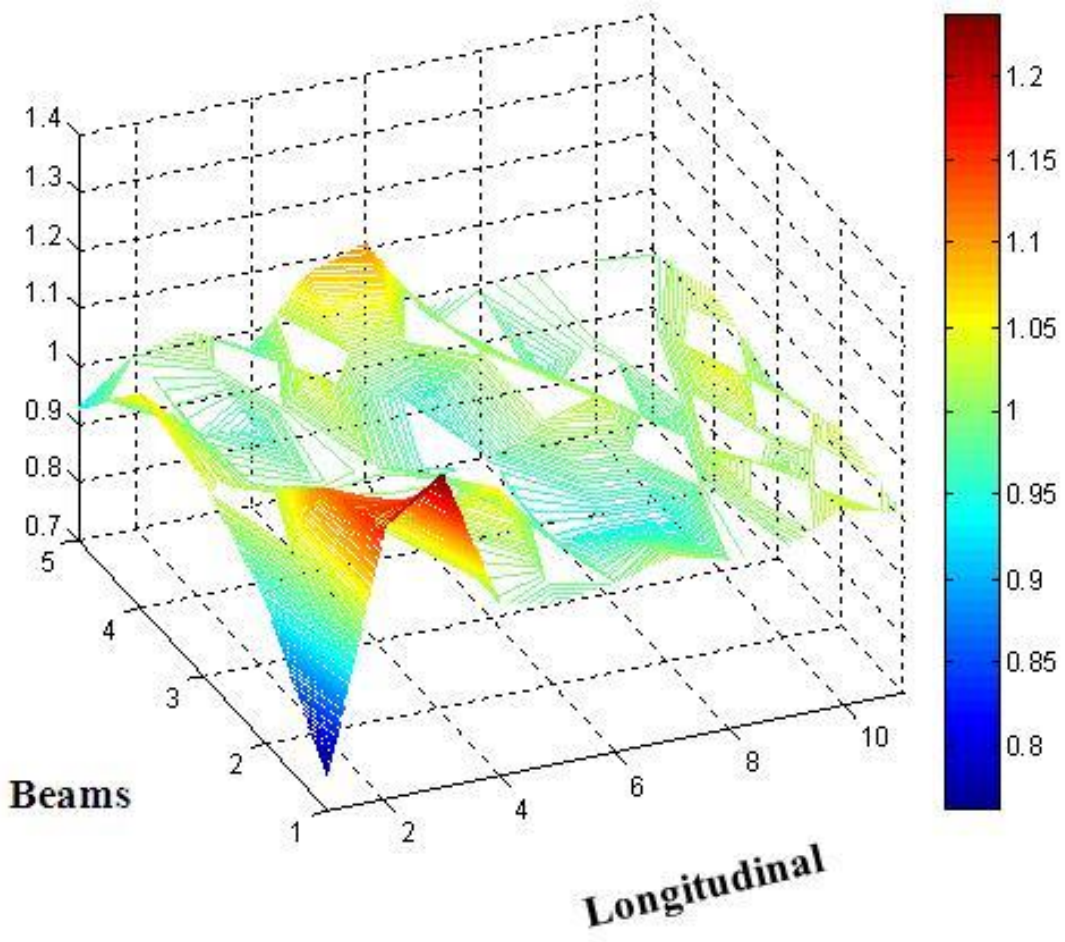

Figure 3.7. Damage index method: damage case 1

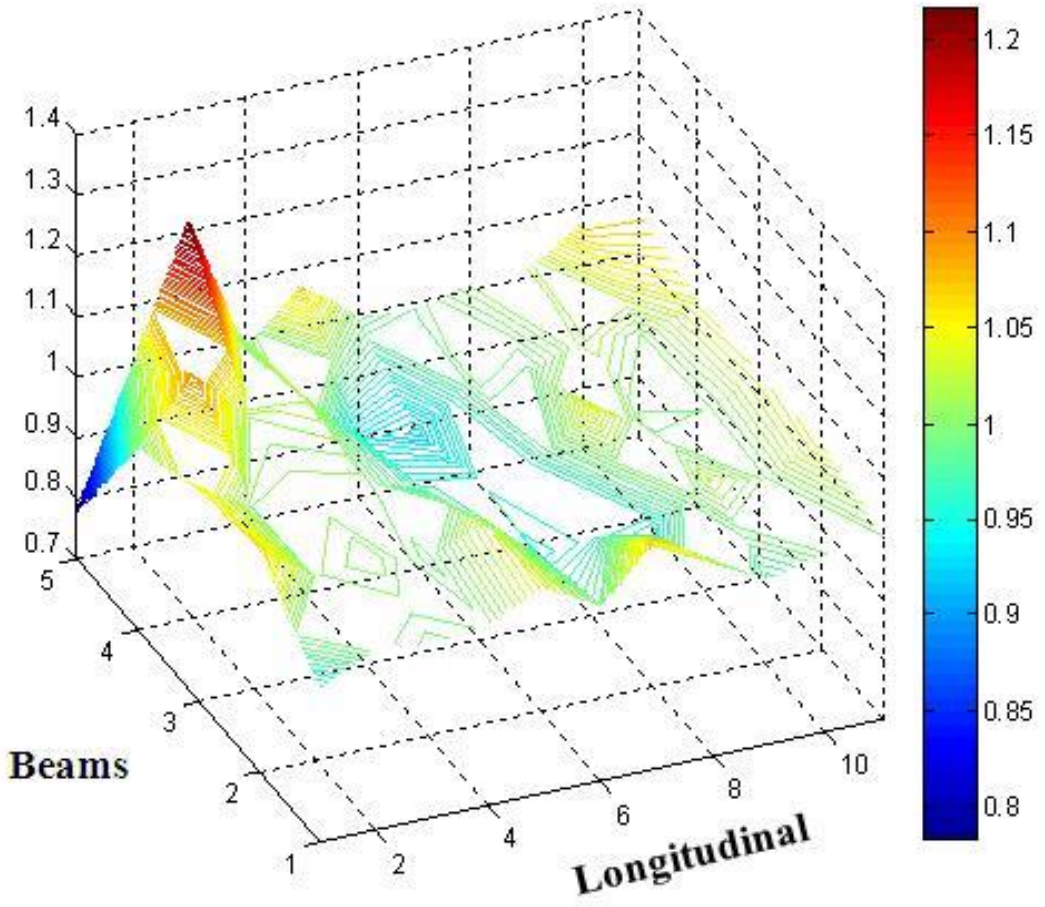

Figure 3.8. Damage index method: damage case 2

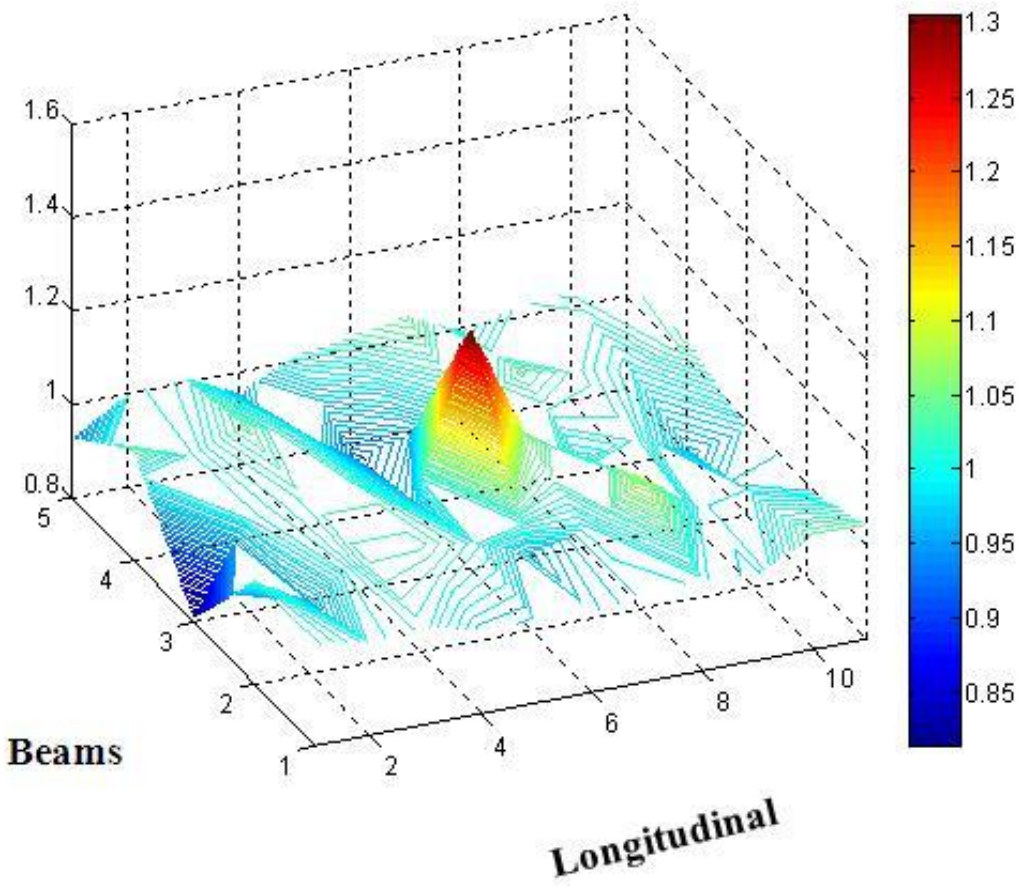

Figure 3.9. Damage index method: damage case 3

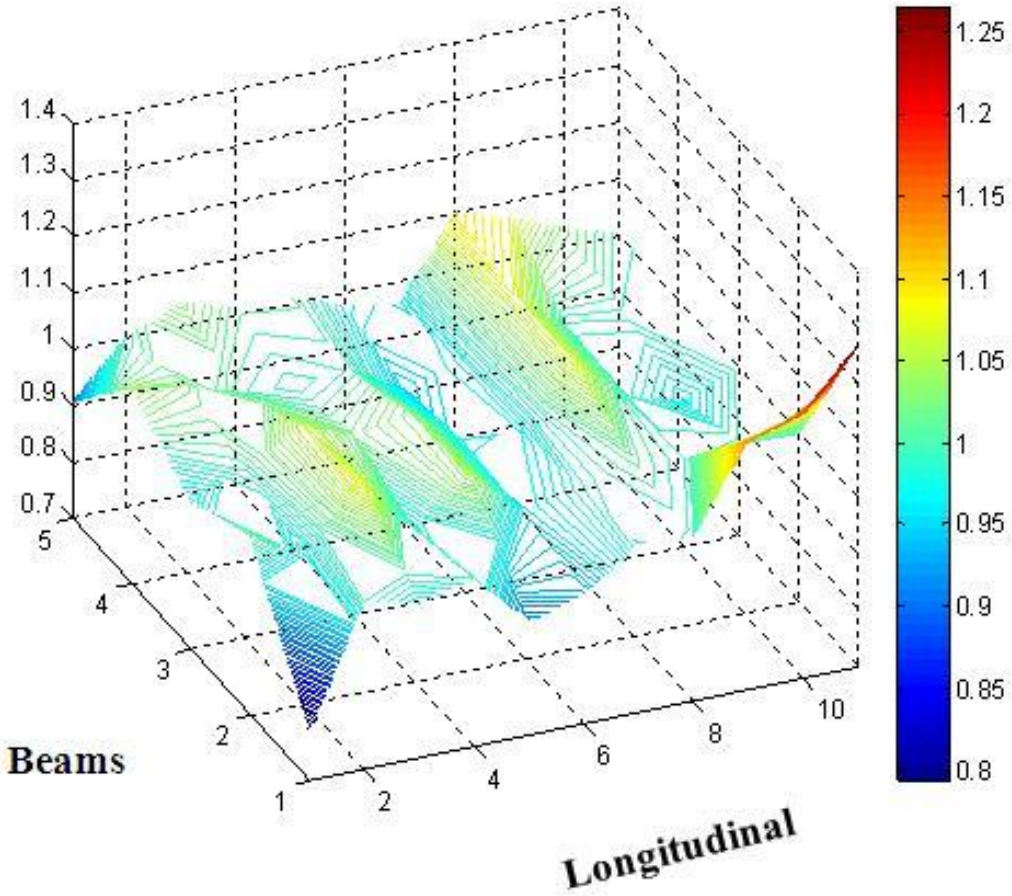

Figure 3.10. Damage index method: damage case 4

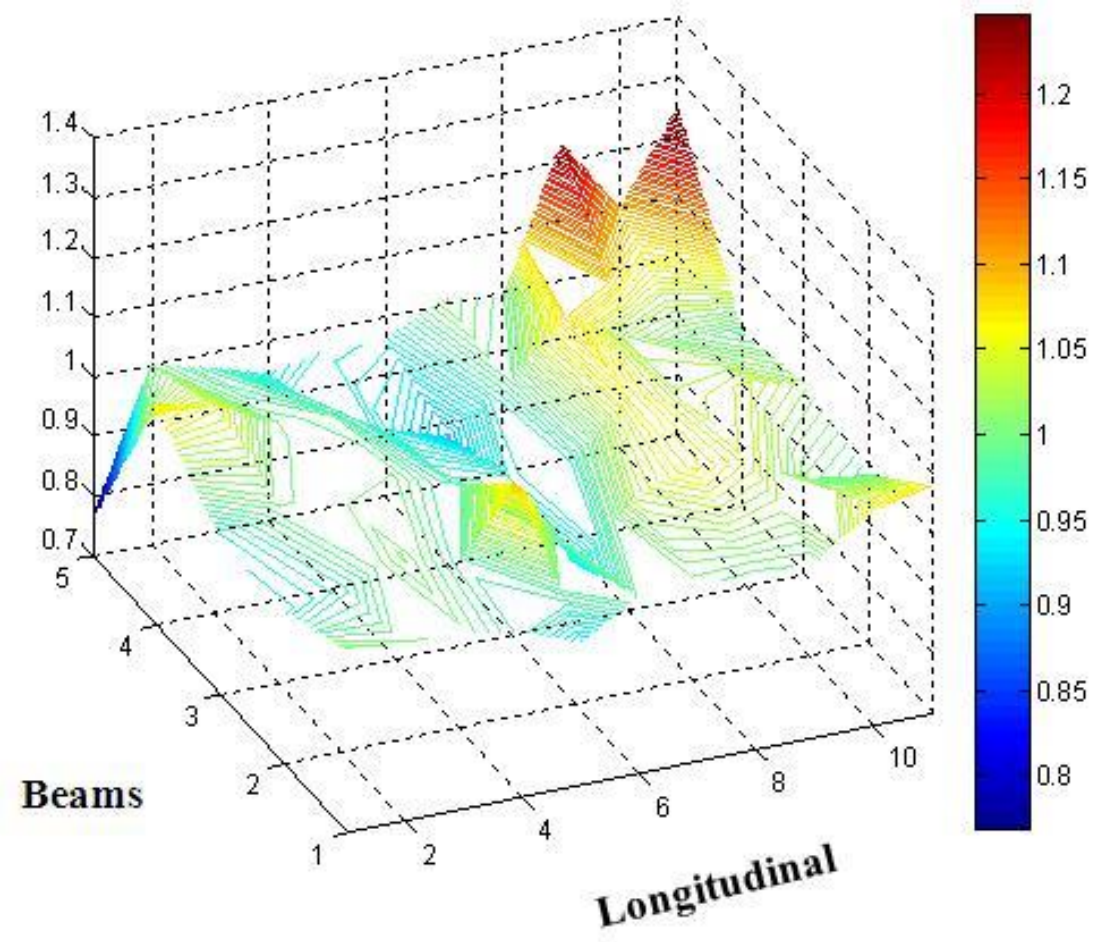

Figure 3.11. Damage index method: damage case 5

3.3. Summary

In this chapter the Modified Curvature Method was proposed as a methodology to locate damage in a bridge structure. This method uses the deflection mode shape data from the developed finite element model. Modeling results were collected for the undamaged state and the five damaged cases. The proposed Modified Curvature Method was then applied to the modal deflection data and combined three dimensional responses of the bridge, including the longitudinal, transverse, and torsional behavior. The Modified Curvature Method results of the undamaged and damaged cases were directly compared to show the change in curvature. This

data was then plotted to graphically show where on the bridge the highest change in curvature was located. The results of the data show a consistent correlation between the location of a high change in curvature and where the damage was simulated in the bridge model.

The Modified Curvature Method was also compared with a previously developed Damage Index method that has been often referenced in other research work over the past twenty years. When comparing the proposed Modified Curvature Method with the Damage Index method it was shown that the Modified Curvature Method is slightly more accurate in identifying the damage location in the bridge model.

4. EXPERIMENTAL VALIDATION OF DAMAGE LOCALIZATION THROUGH THE MODIFIED CURVATURE METHOD

In this chapter an in-lab experiment was built to verify the robustness of the proposed Modified Curvature Method. The experiment was conducted using a small 7 inch by 35 inch steel plate with a thickness of 0.2 inches. The steel plate is a representation of a single span bridge deck. An experimental modal analysis was performed on the steel plate in both undamaged and damaged states. The data obtained was used to verify the suggested Modified Curvature Method in Chapter 3.

4.1. The Steel Plate Model

The steel plate is used to provide a simple representation of a single span bridge deck similar to the bridge used in Chapter 3's numerical analysis. The steel plate is 7.0 inch by 35.0 inch in dimension with a thickness of 0.2 inch. Fixed boundary conditions were applied at the shorter edges, creating a 35.0 inch deck span. Figure 4.1 is a photo of the experimental set up. A measurement grid was applied to the steel plate, which provided 18 impact and measurement locations. Figure 4.2 shows a schematic plot of the measurement grid.

Figure 4.1. Experimental set up

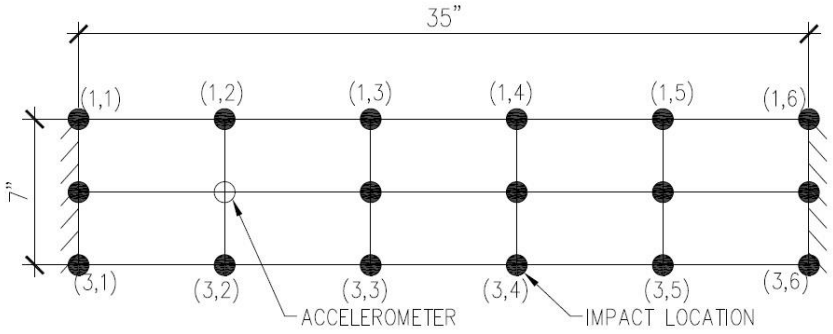

Figure 4.2. Steel plate with measurement grid

4.2. The Instrumentation and Experimental Data Collection

A grid with 18 data points was applied to the surface of the steel plate. An impact hammer was used to produce vibration responses in the steel plate which were then recorded by an accelerometer. The experimental process was conducted by striking the steel plate with the impact hammer at one point while the accelerometer recorded vibration responses at the other points. The impact hammer struck the same location on the steel plate until the accelerometer recorded the vibration responses at all the 18 locations. The impact hammer would then be used to strike another location and the vibration responses were again recorded for all the 18 measurement points. This process was repeated until every combination had been recorded. Being that an impact hammer was used during the experiment, extra care was taken to provide a consistent impact force to obtain quality results.

With all of the data recorded for the undamaged state the experimental data collection could move onto the damaged state. For the damaged state a 0.2” diameter hole was introduced located as shown in Figure 4.3. The same excitation process used for the undamaged state was used with the damaged plate. With the experimental data collection completed, the next step was to perform the data processing.

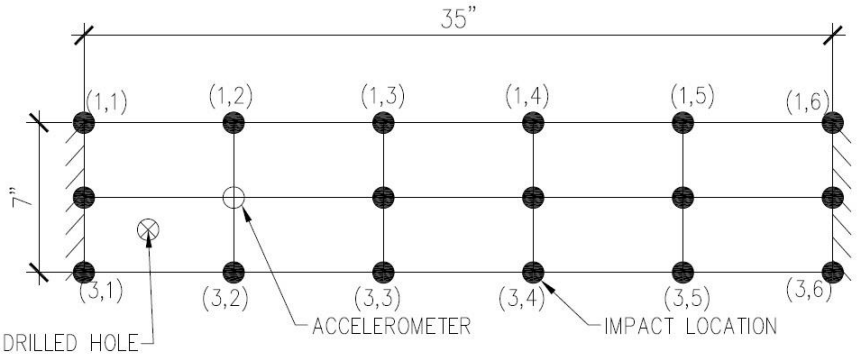

Figure 4.3. Damaged steel plate with measurement grid and damage location

4.3. Experimental Data Processing

With the data collection completed the approach called experimental modal analysis is used to obtain the mode shapes of the steel plate from the frequency data. Mode shapes and frequency are parameters of the natural modes related to responses of a structure under excitation. When damage is introduced to a structure, its stiffness and modal parameters will be affected. These changes to the structure will have an effect on its vibration responses. This in turn can show where the damage is located and the severity of the damage. However, this introduction of damage has a varying effect on the mode shapes, some modes will see a strong effect while others would see a weak effect (Hearn & Testa, 1991). Much research has been done using this experimental data collection approach for the purposes of damage detection in structures.

The initial data obtained from the accelerometer is in the time versus acceleration domain (here the acceleration is in the vertical direction perpendicular to the plate). This data represents the acceleration of the steel plate’s vibrations. The vibration data gives insight into how the steel plate responds to the hammer’s impact force. With the benchmark data of the undamaged steel

plate the comparison to the data from the damaged steel plate will provide an accurate location of the damage.

The next step in the data processing is to calculate the Frequency Response Function (FRF). The FRF is an important measurement in the experimental modal analysis approach. It can be used to directly or indirectly provide important information about a structure. The frequency response function is the ratio of the output response of the structure to the input excitation. The frequency response function for point (1, 1) is shown in Figure 4.4. The high peaks shown from 0 Hz to 600 Hz are indicators of the first seven mode shapes.

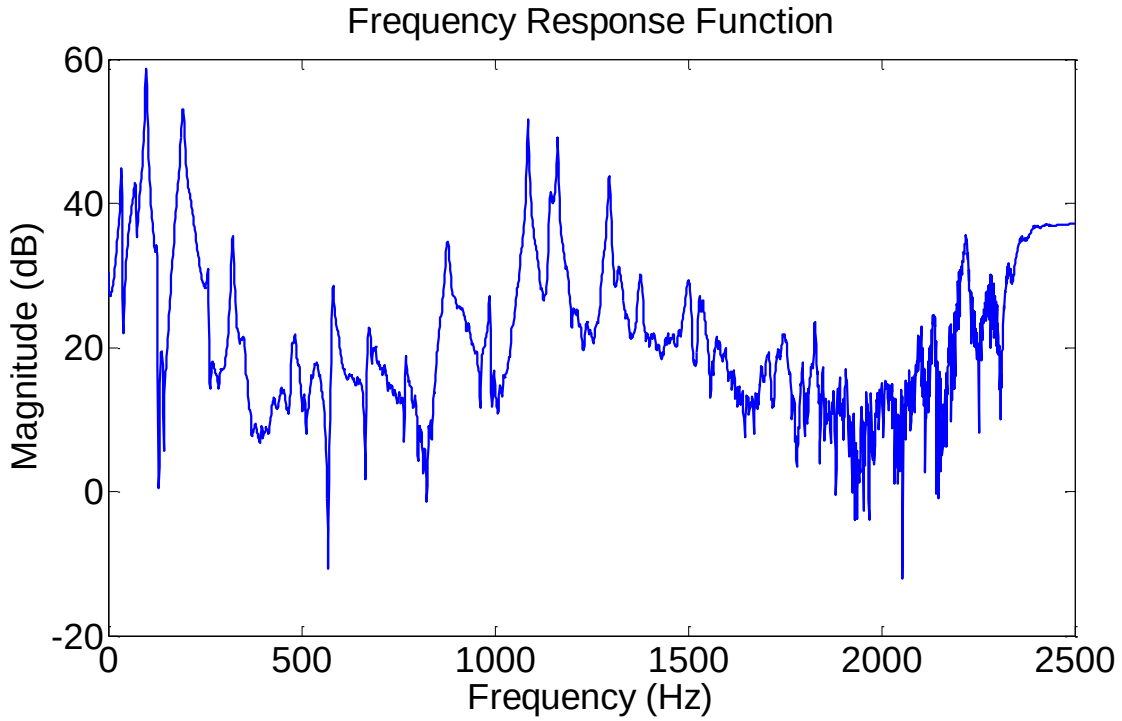

Figure 4.4. Frequency response function at point (1,1)

Next in the experiment data processing is the Complex Mode Indicator Function (CMIF). The CMIF is a numerical tool which has been commonly used in processing experimental data throughout the past 20 years. The CMIF is a simple algorithm based on singular value decomposition (SVD) methods applied to multiple FRF measurements. This function was

developed primarily for FRF data in order to identify the proper number of modal frequencies. The CMIF indicates the existence of real, normal, or complex modes, and the relative magnitude of each mode. Figure 4.5 shows the undamaged state CMIF for the point at (1, 1). The peaks are indicators of mode shapes. However, not all of the peaks are associated with mode shapes. This is due to errors such as noise, leakage, nonlinearity, and a cross eigenvalue effect which can all create apparent peaks (Phillips, Allemaug, & Fladung, 1998). In this analysis, mode one through seven are identified at the following frequencies, 35.4 Hz, 97.66 Hz, 190.4 Hz, 252.7 Hz, 316.2 Hz, and 549.3 Hz, respectively.

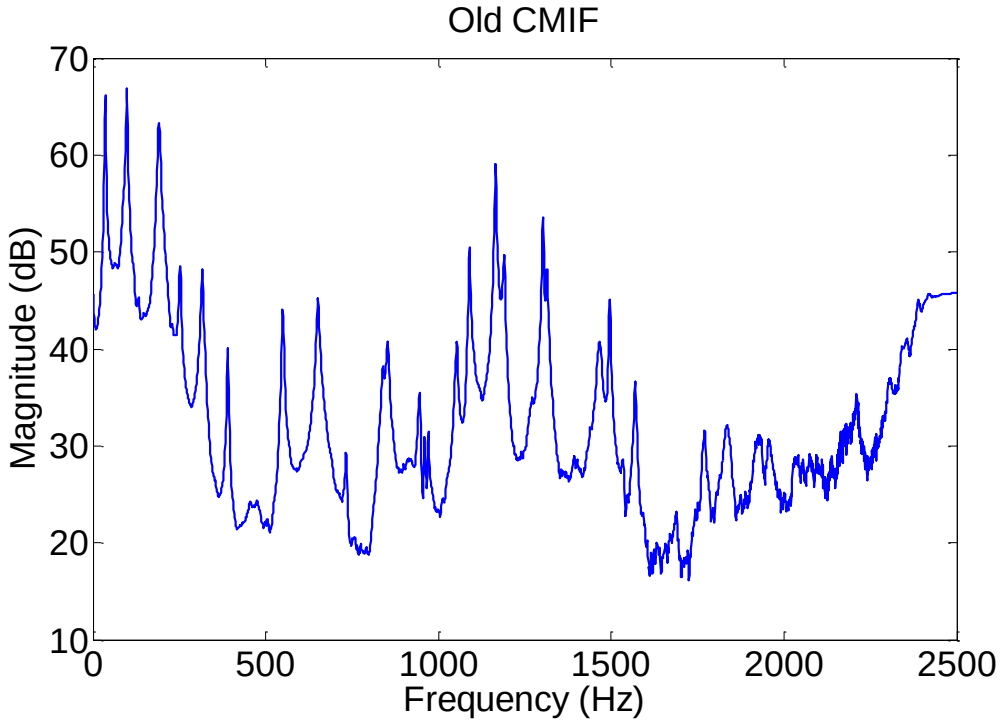

Figure 4.5. CMIF of the undamaged steel plate

Figure 4.6 shows the CMIF of the damaged steel plate. By observation it can be seen that there are changes in the function when comparing to the undamaged CMIF. This result is to be expected since the damage introduced to the steel plate reduces its stiffness. A reduction in stiffness of a structure is expected to have an effect on the mode shapes.

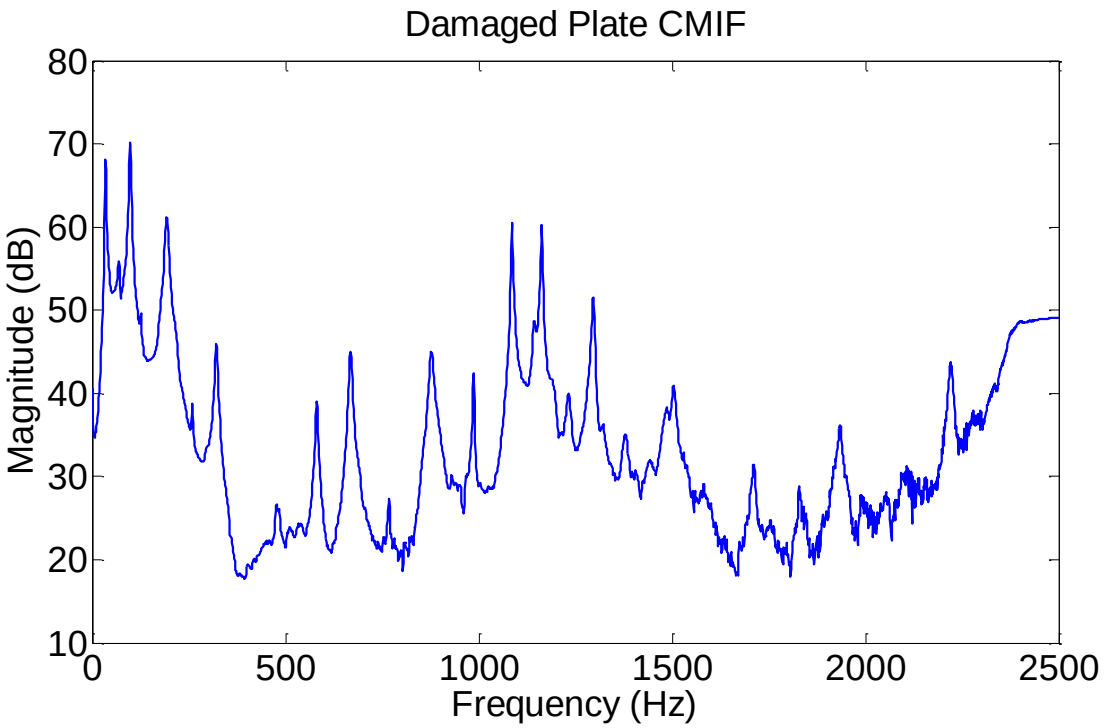

Figure 4.6. CMIF of the damaged steel plate

4.4. Experimental Modal Shapes

The experimental mode shapes have been determined through the CMIF process of the FRF data. As discussed in the previous section the CMIF process was used to identify the experimental mode shapes of the steel plate. The mode shapes were identified at the peaks indicated in plots like those shown in Figure 4.4 and 4.5. The corresponding frequency value of these peaks gives the natural frequency for each mode.

Figure 4.7 below shows mode shape 1 of the undamaged steel plate, which at a frequency of 35.4 Hz. In Figure 4.8, the first mode shape of the damaged steel plate is shown at a slightly lower frequency of 34.18 Hz. It can be seen that the mode shape of the damaged plate has generally the same shape, however there are some slight differences.

Figures 4.7 through 4.18 show the undamaged and damaged experimental mode shapes of modes one through seven. In the other mode shapes it is observed that the damaged mode

shape is significantly different from that of the undamaged steel plate. The frequency of the damaged mode shape also changes, however they could not be used to indicate the damage locations.

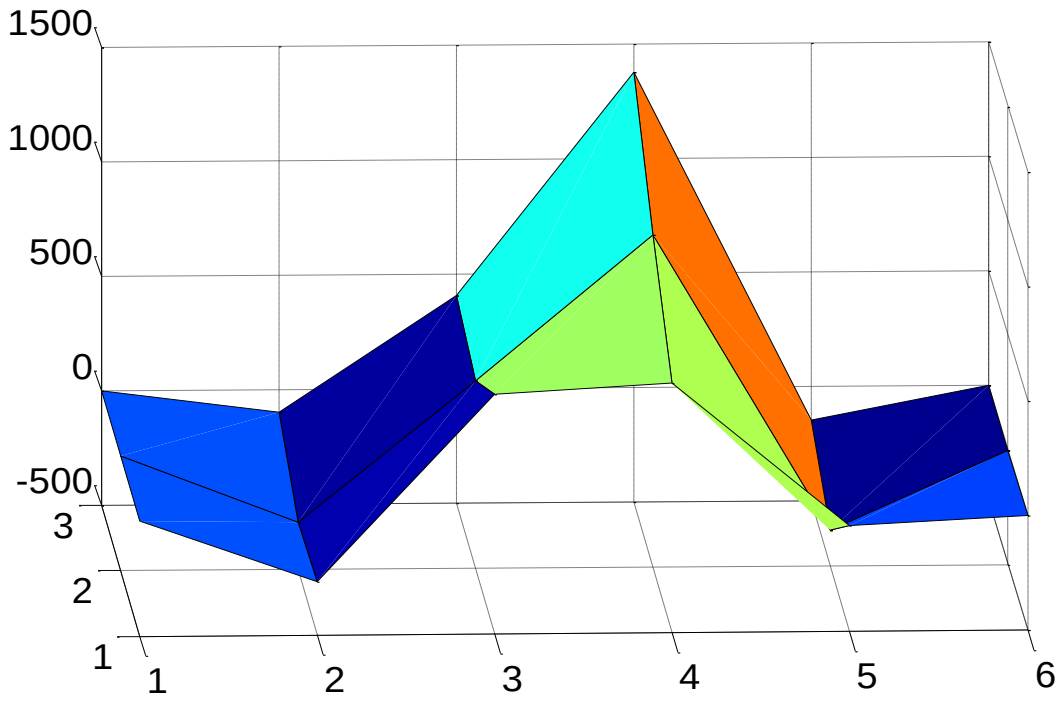

Figure 4.7. Experimental mode shape 1: undamaged steel plate (35.4 Hz)

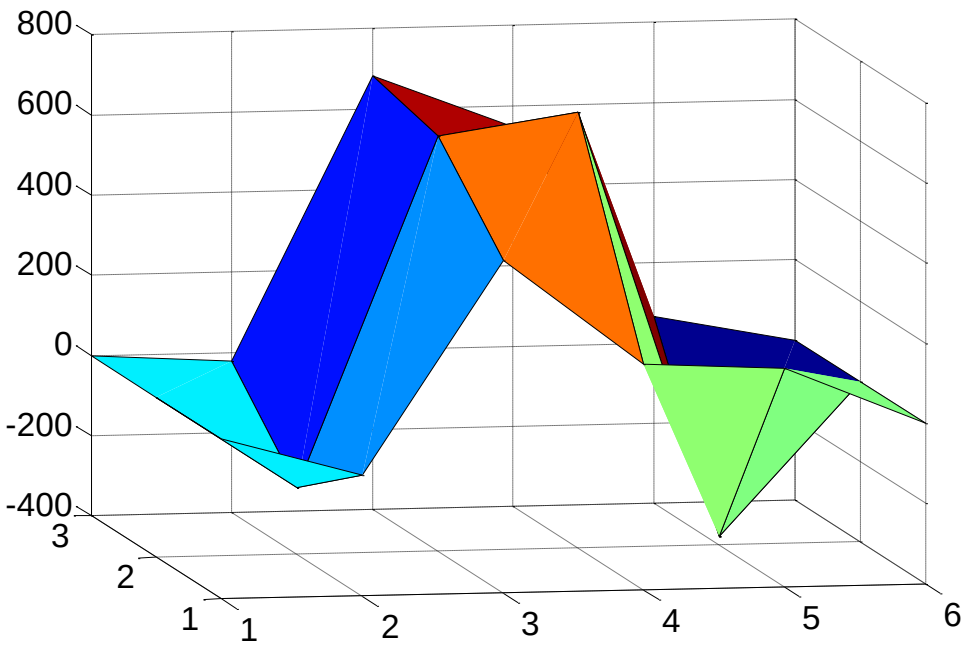

Figure 4.8. Experimental mode shape 1: damaged steel plate (34.18 Hz)

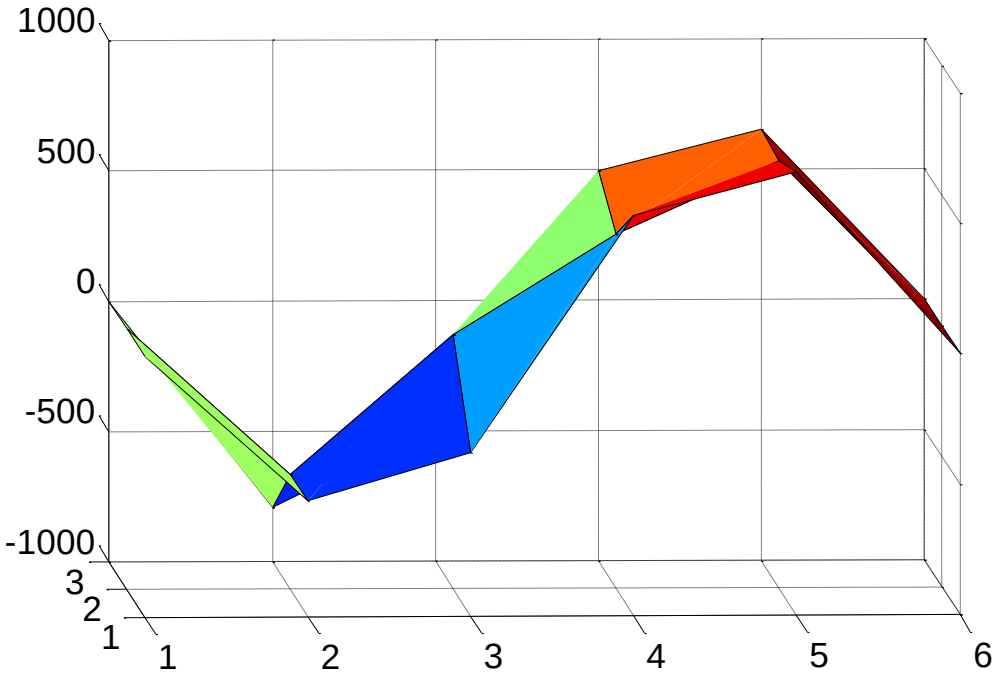

Figure 4.9. Experimental mode shape 2: undamaged steel plate (97.66 Hz)

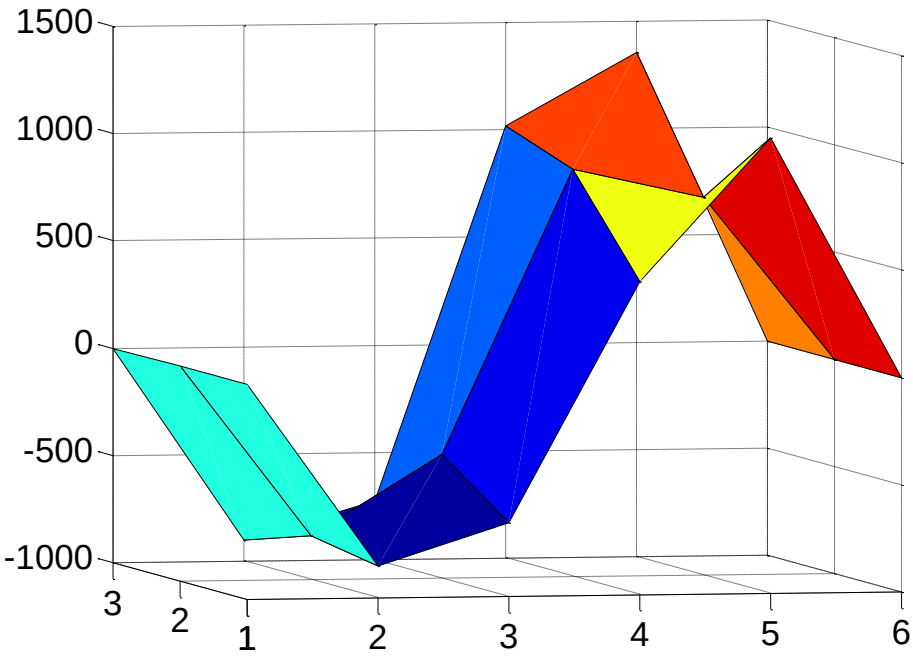

Figure 4.10. Experimental mode shape 2: damaged steel plate (98.88 Hz)

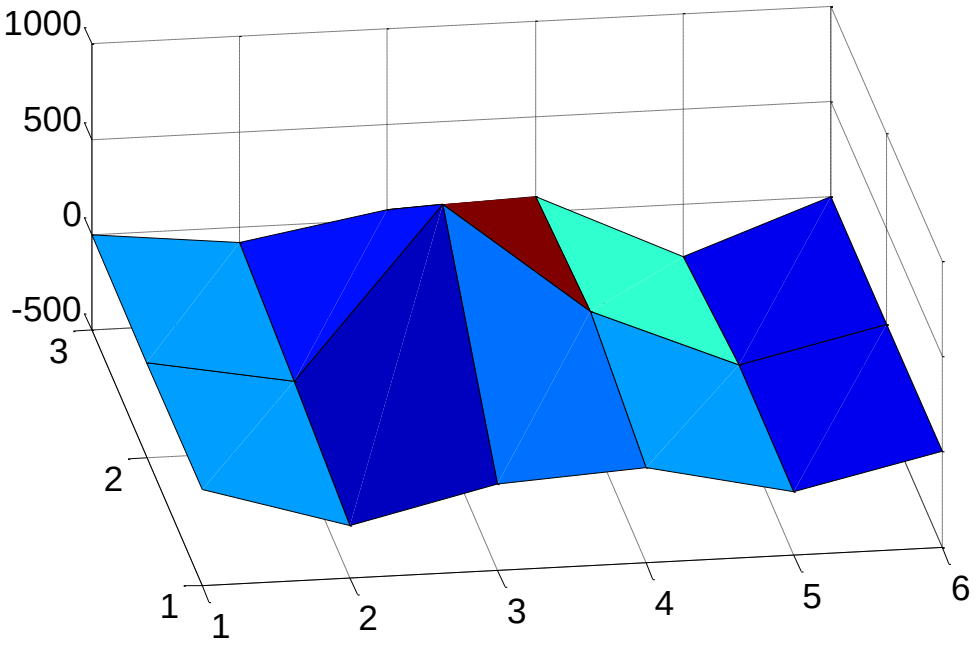

Figure 4.1.1 Experimental mode shape 3: undamaged steel plate (190.4 Hz)

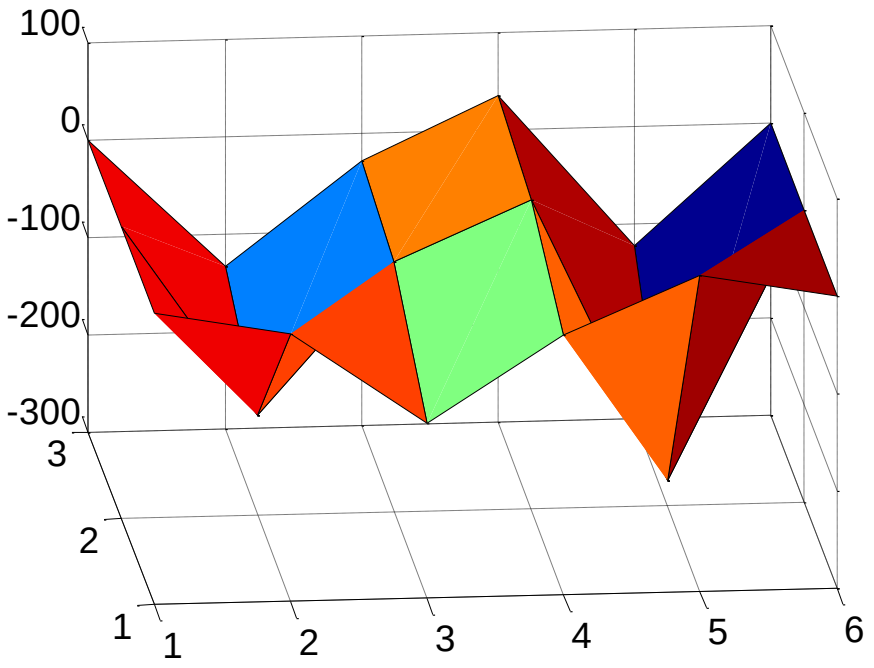

Figure 4.12. Experimental mode shape 3: damaged steel plate (192.9 Hz)

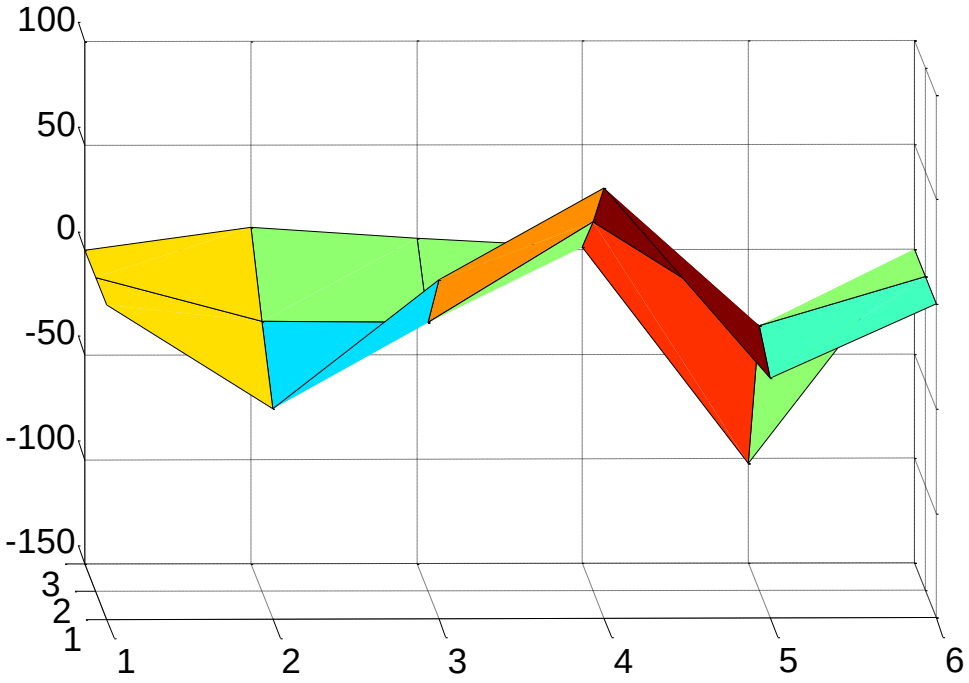

Figure 4.13. Experimental mode shape 4: undamaged steel plate (252.7 Hz)

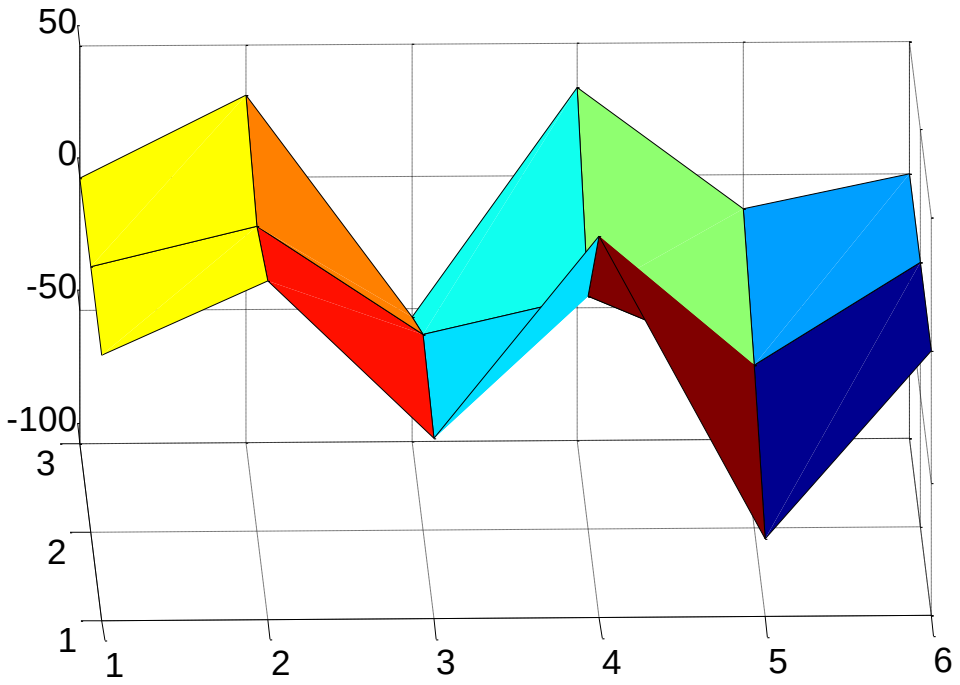

Figure 4.14. Experimental mode shape 5: undamaged steel plate (316.2 Hz)

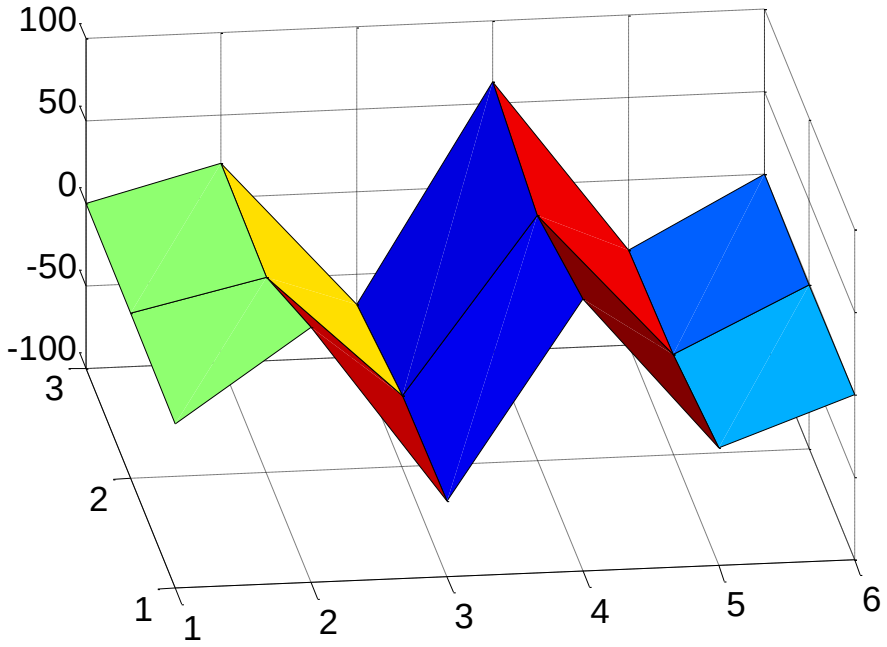

Figure 4.15. Experimental mode shape 5: damaged steel plate (321.04 Hz)

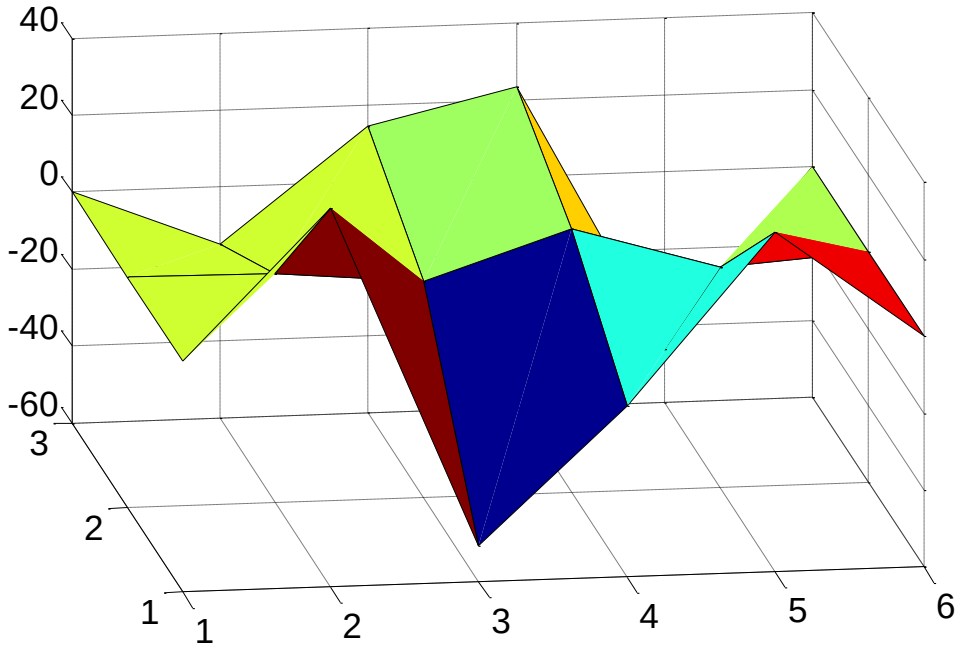

Figure 4.16. Experimental mode shape 6: undamaged steel plate (390.6 Hz)

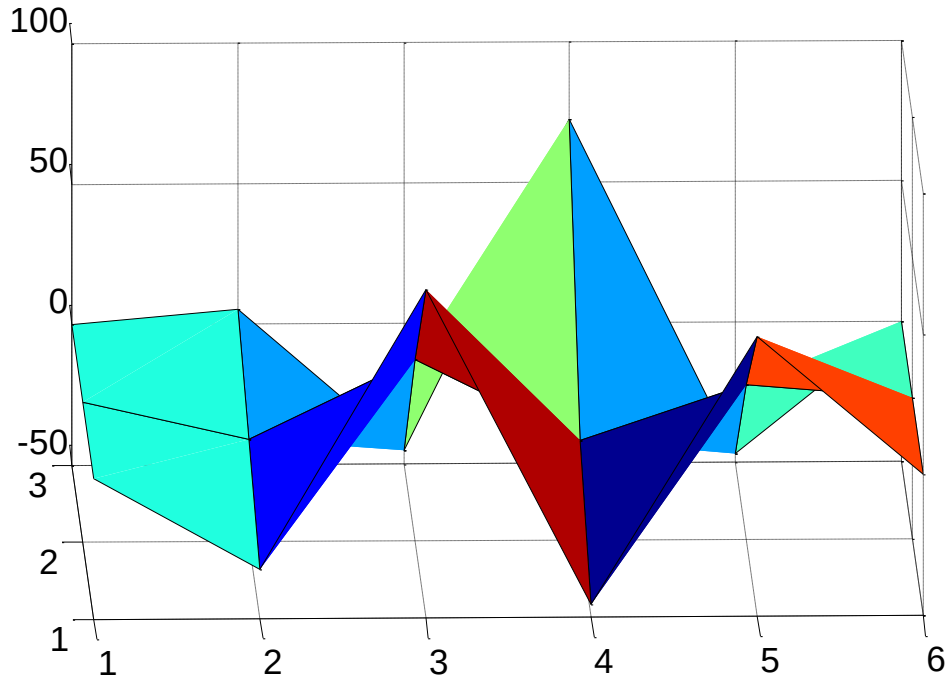

Figure 4.17. Experimental mode shape 7: undamaged steel plate (549.3 Hz)

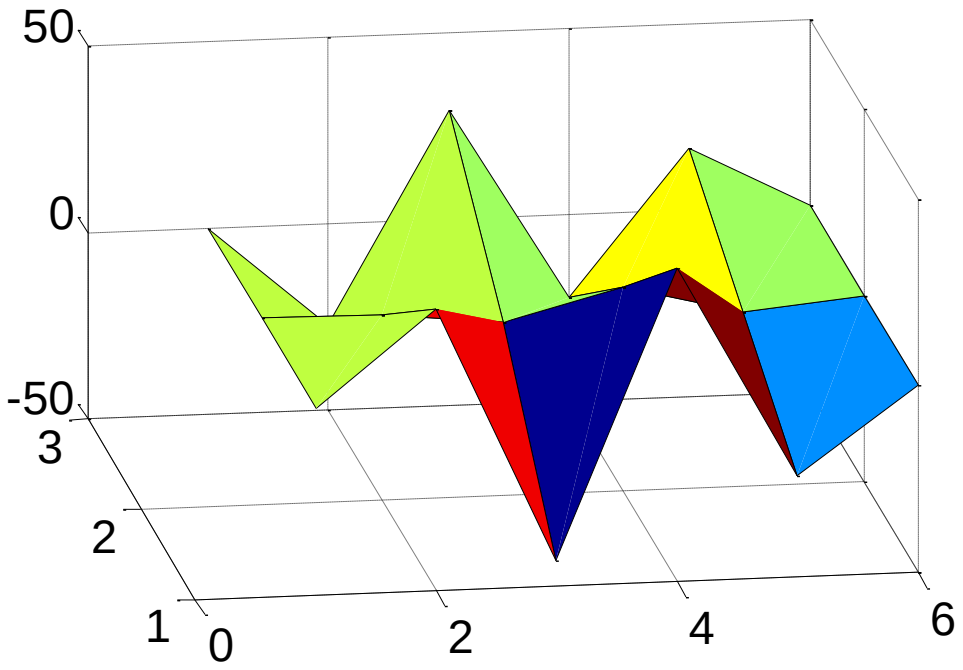

Figure 4.18. Experimental mode shape 7: damaged steel plate (581.1 Hz)

4.5. Experimentally Identified Damage

Using the experimental mode shape data the next step of applying the Modified Curvature Method proposed in Chapter 3 was completed. Repeating the process used in Chapter 3 and using the difference of the damaged structure's composite curvature over the undamaged structure's composite curvature, the approximate damage location can be determined.

Figure 4.19 shows the results of applying the Modified Curvature Method to the experimental mode shape data. The difference of the damaged composite curvature and the undamaged composite curvature, summarizing all the detectable modes (mode 1, 2, 3, 5 and 7), is presented with a surface plot using MATLAB. By observation it can be seen that the surface plot has two peaks. The low peak, located at the measurement point (3, 2) indicates the damage location. However, a similar peak of positive magnitude is shown at the opposite side of the surface plot. This peak is a false indicator. Even with a false indication of damage, the correct

damage location has been identified. For practical purposes, this would be sufficient in an actual bridge inspection because the bridge professional would only need to focus inspection efforts at two locations. This prevents the need for an exhaustive inspection effort of the entire bridge, which would lead to more efficient use of time and resources.

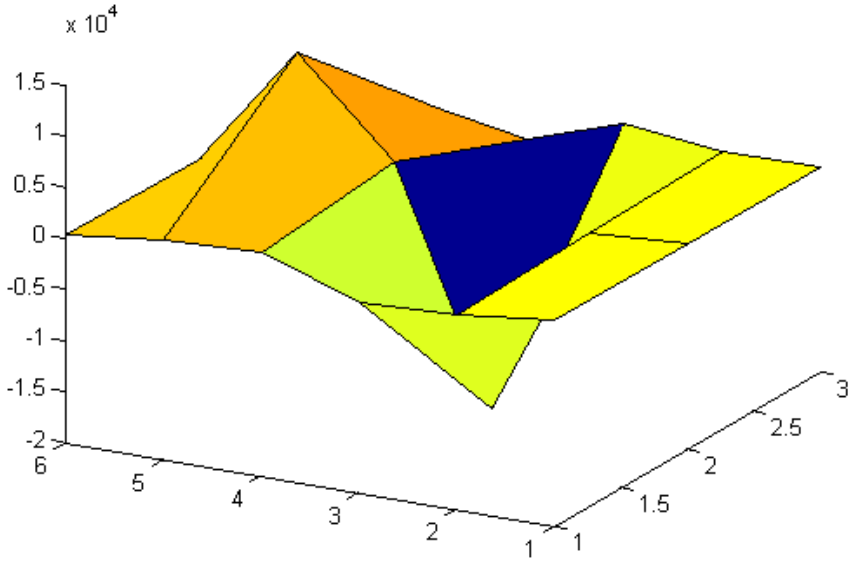

Figure 4.19. Damage localization with the modified curvature method

4.6. Summary and Conclusions

In this chapter an in-lab experiment using a thin steel plate to represent a bridge deck was used to verify the accuracy of the proposed damage detection method in Chapter 3. An impact hammer was used to create excitations in the form of vibration which were recorded with an accelerometer. The accelerometer provided the time versus acceleration data which could be then processed to determine the frequency response function. The FRF was further processed using the Complex Mode Indication Function to determine the experimental mode shapes of the

undamaged and damaged steel plate. With the experimental mode shapes determined, the Modified Curvature Method was applied to the data to determine the damage location.

Using the experimental mode shape data and applying the Modified Curvature Method to determine the damage location, as was discussed in the previous section, the proposed damage detection method show the ability to locate the damage in the steel plate. However, the process also yielded a false damaged location as an asymmetrical peak. This asymmetrical peak was also found with the numerical data used in Chapter 3. Even with this false indicator the ability of the Modified Curvature Method to locate damage accurate is verified through the in-lab experiment conducted in this chapter.

5. CONCLUSIONS AND FUTURE WORK

5.1. Conclusions

In this thesis, an innovative bridge health monitoring methodology is proposed to identify the bridge status. First a field load testing is carried out under Bridge Diagnostics, Inc. and the data collected was used to verify a numerical grillage model for bridges. Based on the verified numerical model, the modified curvature method is proposed to relate the damage status with the curvature changes. Finally the suggested modified curvature method is verified through an in-lab experiment. The in-lab experimental modal analysis verified the modified curvature method concept and located the damage successfully.

In summary, the thesis studied,

1. Model slab on girder bridges through the Grillage method. Through the verification from the field testing data, the created grillage model could be used further for bridge damage assessment.
2. Through stiffness reduction to mimic damage in bridges, a modified curvature method is proposed to include bending and twisting effect into damage assessment and the proposed method successfully located the damages in bridges.
3. Through an in-lab experiment, the suggested modified curvature method was verified through the experimental data and experimental modal analysis. The verified methodology could be integrated in bridge element or system rating in future.

5.2. Future Work

In the future, efforts will be made to improve the damage detection capabilities and reduce the possibility of false indicators. It was planned to execute an in-lab experiment on a scaled down bridge model with damage applied to various structural elements, such as bearing, bend caps, piers, etc. However due to the time limits in the Master program, it will be put into future works for improvements.

Another extension of the method could lie in relating the modified curvature with the load rating of bridge elements and the whole bridge. It has been initiated in this research at a preliminary level and will be explored further in future.

REFERENCES

Al-Saidy, A. H., Klaiber, F. W., Wipf, T. J., Al-Jabri, K. S., & Al-Nuaimi, A. S. (2008, May). Parametric study on the behavior of short span composite bridge girders strengthened with carbon fiber reinforced polymer plates. *Construction and Building Materials, 22*(5), 729-737.

Amer, A., Arockiasamy, M., & Shahawy, M. (1999, August). Load Distribution of Existing Solid Slab Bridges Based on Field Tests. *Journal of Bridge Engineering, 4*(3), 189-193.

American Society of Civil Engineers. (2013). *2013 Report Card for America's Infrastructure*. Retrieved November 2014, from Infrastructure Report Card: http://www.infrastructurereportcard.org/a/#p/bridges/

Bonessio, N., Lomiento, G., & Benzoni, G. (2012). Damage identification procedure for seismically isolated bridges. *Structural Control and Health Monitoring, 19*(5), 565-578.

Bridge Diagnostics, Inc. (2012). *Field Testing and Load Rating Report: Bridge 09-125-16.0 Over Rush River Cass County, ND.*

Crawford, R., & Ward, H. (1964). Determination of the natural periods of buildings. *Bulletin of the Seismological Society of America, 54*(6A), 1743-1756.

Cusens, A., & Pama, R. (1975). *Bridge Deck Analysis.* London: Wiley.

Dohler, M., Hille, F., Mevel, L., & Rucker, W. (2014). Structural health monitoring with statistical methods during progressive damage test of S101 Bridge. *Engineering Structures, 69*, 183-193.

Farrar, C., & Jauregui, D. (1996). *Damage Detection Algorithms Applied to Experimental and Numerical Modal Data from the I-40 Bridge.* Los Alamos, New Mexico: Los Alamos National Laboratory.

Hearn, G., & Testa, R. (1991). Modal Analysis for Damage Detection in Structures. *Journal of Structural Engineering, 117*(10), 3042-3063.

Hillis, A., & Courtney, C. (2011). Structural health monitoring of fixed offshore structures using the bicoherence function of ambient vibration measurements. *Journal of Sound and Vibration, 330*(6), 1141-1152.

Hudson, D. (1977). Dynamic Tests of Full-Scale Structures. *Journal of the Engineering Mechanics Division, 103*(6), 1141-1157.

Iwasaki, T., Penzien, J., & Clough, R. (1972). *Literature survey - Seismic effects on highway bridges.* University of California, College of Engineering. Springfield, Virginia: National Technical Information Service.

Jaeger, L., & Bakht, B. (1982). The grillage analogy in bridge analysis. *Canadian Journal of Civil Engineering*, 224-235.

Kessler, S., Spearing, S., & Soutis, C. (2002). Damage detection in composite materials using lamb wave methods. *Smart Materials and Structures, 11*(2), 269-278.

Kim, J.-T., & Stubbs, N. (1995). Model-uncertainty impact and damage detection accuracy in plate girder. *Journal of Structural Engineering*, 1409-1417.

Lu, P., & Shao, C. (2012). Simplified analysis of a skew-plate bridge based on grillage analogy model. *The IES Journal Part A: Civil & Structural Engineering, 5*(4), 253-262.

McLamore, V. (1971). Ambient Vibration of Two Suspension Bridges. *Journal of the Structural Division, 97*(10), 2567-2582.

Meng, J. Y., & Lui, E. M. (2002, May). Refined Stick Model for Dynamic Analysis of Skew Highway Bridges. *Journal of Bridge Engineering, 7*(3), 184-194.

Nichols, J. (2003). Structural health monitoring of offshore structures usign ambient excitation. *Applied Ocean Research*, 101-114.

Oehler, L. (1957). *Vibration susceptibilities of various highway bridge types.* Report 272, Michigan State Highway Department, Testing and Research Division.

Phillips, A. W., Allemaug, R. J., & Fladung, W. A. (1998). The Complex Mode Indicator Function (CMIF) as a parameter estimation method. *The International Society for Optical Engineering, 1*.

Rowe, R. (1962). *Concrete Bridge Design.* London: CR Books.

Samali, B., Choi, F., & Crews, K. (2010). Application of the damage index method for plate-like structures to timber bridges. *Structural Control and Health Monitoring, 17*(8), 849-871.

Srinivasan, M., Kot, C., Hsieh, B., & Chung, H. (1981). Dynamic testing of as-built nuclear power plant buildings: An evaluative review. *Nuclear Engineering and Design*, 97-115.

Varney, R. (1966). *The dynamic of a single span prestressed concrete box-beam highway bridge.* Fritz Laboratory Reports.

Ward, H. S., & Crawford, R. (1966, August). Wind-induced vibrations and building modes. *Bulletin of the Seismological Society of America, 56*(4), 793-813.

Wipf, T. J., Phares, B. M., Doornink, J. D., Greimann, L. F., & Wood, D. L. (2007). *Evaluation of Steel Bridges (Volumn I): Monitoring the Structural Condition of Fracture-Critical Bridges using Fiber Optic Technology*. Iowa State University. Bridge Engineering Center.